

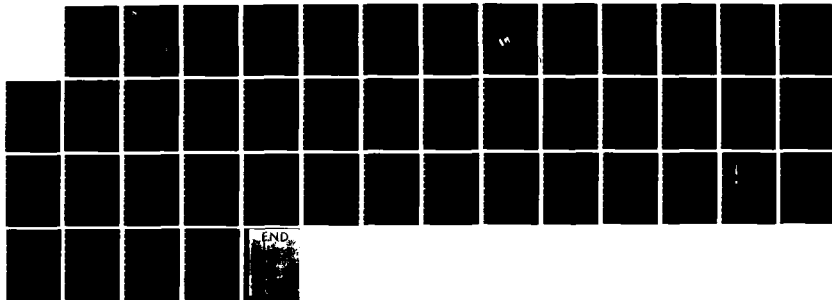
AD-A136 685

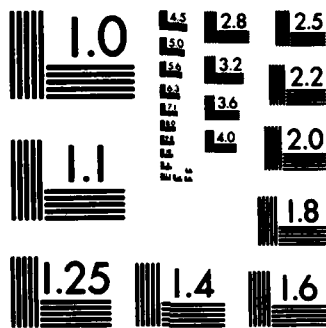
OPTICAL SETTLING TUBE(U) SEA TECH INC CORVALLIS OR
R BARTZ ET AL. 21 NOV 83 OST-REF-11-83 N00014-83-C-0734

1/1

UNCLASSIFIED

F/G 14/2 NL





MICROCOPY RESOLUTION TEST CHART
NATIONAL BUREAU OF STANDARDS-1963-A



SEA TECH, INC.

P.O. Box 779 • Corvallis, Oregon 97339 • (503) 757-9716

12

AD A136685

OPTICAL SETTLING TUBE
FINAL REPORT TO THE OFFICE OF NAVAL RESEARCH
FOR
CONTRACT NUMBER N00014-83-C-0734

BY
ROBERT BARTZ AND J. RONALD V. ZANEVELD

OST Ref. 11-83
November 1983

DTIC
ELECTED
S JAN 11 1984
A

DTIC FILE COPY

Approved:

Robert Bartz

Robert Bartz, President
Sea Tech Inc.

This document has been approved
for public release and sale; its
distribution is unlimited.

83 12 19 198

TECHNICAL REPORT STANDARD TITLE PAGE

1. Report No. OST Ref. 11-83	2. Government Accession No. AD-A136685	3. Recipient's Catalog No.
4. Title and Subtitle OPTICAL SETTLING TUBE FINAL REPORT		5. Report Date 21 NOV, 1983
7. Author(s) R. BARTZ / J.R.V. ZANEVELD		6. Performing Organization Code
9. Performing Organization Name and Address SEA TECH INC. P.O. BOX 779 CORVALLIS, OR 97339		8. Performing Organization Report No.
12. Sponsoring Agency Name and Address CDR J.J. SPIGAI, ONR, CODE 425GG 800 NORTH QUINCY STREET ARLINGTON, VIRGINIA 22217		10. Work Unit No.
15. Supplementary Notes		11. Contract or Grant No. N00014-83-C-0734
16. Abstract A laboratory model Optical Settling Tube referenced in appendix 1 has been redesigned to obtain in situ settling velocity distributions in the deep ocean. A prototype instrument was constructed and tested on a HEBBLE cruise in June, 1983. The instrument functioned perfectly and in situ settling velocity distributions in the deep ocean were measured. Data listed in this report demonstrates that an Optical Settling Tube can now be used for the purpose of repeatedly measuring settling velocity distributions in the deep ocean from a moored platform.		13. Type of Report and Period Covered FINAL REPORT FY 1983
17. Key Words (Selected by Author(s)) HEBBLE OPTICAL SETTLING TUBE TRANSMISSOMETER SETTLING VELOCITY		14. Sponsoring Agency Code N-00014
19. Security Classif. (of this report) U		18. Distribution Statement
20. Security Classif. (of this page)		21. No. of Pages 43
22. Price A1		23. Distribution/Availability Codes and/or Special

Accession For

DTIC

NTIS

Unannounced

Autism file

Distribution/Availability Codes

and/or Special

*For sale by the Clearinghouse for Federal Scientific and Technical Information, Springfield, Virginia 22151.



INTRODUCTION

Under contract number N00014-83-C-0734 with the Office of Naval Research, Sea Tech Inc. agreed to build a prototype Optical Settling Tube, (OST) and to field test the instrument.

The theory behind the operation of the instrument has been set forth in Zaneveld et. al. (1982), which is included as appendix 1 of this report. In Zaneveld et. al. (1982) it was shown that if one measures the beam attenuation coefficient, (c) as a function of time in a closed tube, filled with a homogeneous hydrosol, it is possible to derive a settling velocity distribution, (SVD). If the specific gravity of the material in suspension is known the particle size distribution and the concentration weighted settling velocity for the sample can also be calculated.

The primary task under this contract was to redesign a proven laboratory OST and make it operational under deep sea conditions, without loss of the scientific viability of the data.

DESIGN CRITERIA

The instrument was redesigned so that it could repeatedly (at 24 hour intervals) measure the SVD, from a moored tripod. Since this was a prototype, the instrument was not designed for long deployments, but could be expected to operate for continuous deployments of several days. An appropriate closing mechanism had to be designed, which would consume little power and which adequately isolated the interior of the tube from the outside environment.

The settling tube itself has to be designed so that when the tube was open, the interior of the tube would equilibrate with the exterior environment in a reasonably short period of time.

DESIGN

The prototype USI was designed to function in water depths of 5000 meters for a period of several days to obtain particle settling velocity data. The settling tube was designed to provide a 25 cm column height, the path length for the transmissometer was 25 cm, and the tube was 10 cm wide. The transmissometer is described by Bartz et. al. (1978) in appendix 2. The transmissometer was modified only to the extent necessary to mount it on the settling tube.

The opening and closing mechanism of the settling tube consists of a low current drain stepping motor which slowly opens the top and bottom lids against a spring. When the lids are fully open the tube is allowed to flush for a period of two hours, at the end of this period a clutch releases and the lids snap closed (within two seconds in water). The suspended material in the tube is then allowed to settle out for twenty two hours after which the procedure is repeated.

The OST was mounted on a tripod constructed by Mr. F. Hess at WHOI (figure 1A). The instrument height above the base was 0.75 meters, (measured from the base to the top lid).

DEPLOYMENT

The prototype OST was deployed on the HEBBLE cruise during June of 1983. Due to other priorities on this cruise the prototype OST was only deployed for two days. Deployment was on 13 June, 1983 at 0137Z and recovery was on 15 June, 1983 at 0723Z. Preliminary data from this deployment was analyzed on board. Due to the excellent results of the first deployment, WHOI scientists urged Sea Tech Inc. to deploy the prototype OST for three months starting at the end of the cruise. Despite some misgivings on the part of Sea Tech Inc., due to the very limited trial deployment and the limited data capacity of the recorder borrowed from Oregon State University, it was agreed to moor the prototype OST for three months on the WHOI tripod designed by Mr. F. Hess. The Oregon State University data recorder was modified aboard ship to accept three months of data. This necessitated decreasing the sampling interval to once every four minutes, degrading the size resolution at the large end of the size distribution.

The WHOI tripod, the prototype OST and the OSU data recorder were subsequently lost when the release mechanism of the WHOI tripod failed to operate properly.

PERFORMANCE

As a result of the above only two days of data are available to evaluate the performance of the prototype OST.

Primary concerns in the evaluation are:

- 1) Does the settling tube flush adequately, so that the sample obtained is representative of the water outside of the tube.
- 2) Does the closing mechanism properly isolate the interior of the tube from the exterior so that all "crosstalk" is avoided.

As a primary evaluation tool we used a second beam transmissometer mounted on the outside of the OST. In this manner it was possible to determine equilibration time as well as monitor the outside environment while the interior particles were settling out.

Figure 1 shows the interior and exterior beam attenuation coefficient (c) while the instrument is being lowered to the ocean bottom. During the down cast the closing mechanism is left open. Calibration of both transmissometers was accomplished by setting c equal to 0.37 when the instrument measured the cleanest water during the down cast, (5.9 to 6.0 hours). It can be seen that the exterior and OST beam attenuation coefficients agree to within 0.01 /M during the rest of the cast, (0.01/M corresponds to approximately 10 micrograms per liter particle concentration).

Figure 2 shows data from one-half hour before the tripod touches bottom to two hours after it has landed. During the entire period shown the OST lids are open. During the first half hour of this figure the OST is falling through the water column. Clearly visible is a bottom nepheloid layer with an intensity of 0.35 /M. It should also be noted that the interior and exterior transmissometers track perfectly through the nepheloid layer. A cloud of sediment is thrown up as the instrument tripod touches bottom. This cloud clears first in the exterior transmissometer and approximately ten minutes later in the interior. For the remainder of the two hours the two transmissometers track very closely. It is thus shown that the equilibration time of the settling tube is approximately ten minutes, although this should vary depending on current velocity. The current velocity for this time period was measured by Dr. A. Williams on a different tripod. Dr. Williams estimated that the current velocity in the location of the OST tripod was between three and eight cm/sec during the two day period that the OST was moored.

The prototype OST is designed to operate on a 24 hour cycle, 2 hours of which the tube is left open to equilibrate, after which the tube is closed and the transmission is monitored for 22 hours, after which the cycle is repeated.

Figure 3 shows the first operational cycle of the OST, several features are of interest. The exterior beam attenuation shows high frequency variations with an amplitude of about 0.02 /M (approximately 20 micrograms per liter). The interior beam attenuation shows no such high frequency fluctuations, showing that high frequency turbulence outside the tube does not penetrate inside.

The beam attenuation inside the OST generally declines as a function of time. In theory the beam attenuation should decrease continuously once the tube is closed, if the initial sample is well-mixed and if there are no outside influences. It is seen that after a steady decrease for the first nine hours there are several fluctuations on the order of 0.02 /M from nine hours onward. How these fluctuations are generated is not understood at present and is something that should be studied in the future. Possible causes are inhomogeneities in the original sample and disturbances of the fiberglass tripod. The fluctuations are probably not due to external changes in beam attenuation since fluctuations inside are often out of phase with outside fluctuations such as from nine to eleven hours.

The last two hours show the beam attenuation as the tube is opened. Again the interior and exterior beam attenuation converge rapidly which shows good flushing characteristics of the tube and excellent tracking between the two transmissometers.

Figure 4 is an enlargement of the two hour tube open period. It can be seen that the flushing time of the tube is approximately twenty minutes for nearly perfect tracking between the inside and outside transmissometers.

Figure 5 shows the second complete sampling sequence of the OST. The same general features are apparent. The beam attenuation generally decreases, the exterior turbulence is much greater than the interior, and the interior signal shows low frequency fluctuations with an amplitude of less than $0.02/M$. Notice again that the rapid decrease in exterior beam attenuation at ten hours does not coincide with a similar decrease in the interior. During the second day the initial beam attenuation was lower, and the subsequent decrease was less. Upon opening of the tube the interior and exterior equilibrated rapidly again.

Figure 6 shows the sequence from opening of the tube through release of the tripod at 23.6 hours. Figure 7 shows the release and the subsequent upcast. It is seen that the interior and exterior beam attenuations agree very well. Comparing the down cast (figure 1) with the upcast (figure 7) it is seen that the instrument is stable within $0.01/M$ or about 10 micrograms per liter from launch to recovery.

Figure 7 and 8 show the natural logarithm, (\ln) of settling time vs percent transmission, (t) for the two settling sequences. Because of Stokes law, $(\ln t)$ is proportional to $(\ln d)$ so that the lower scale is proportional to the (\ln) of diameter, (d) . Whenever the slope of transmission vs $(\ln t)$ is large a maximum in the settling velocity distribution is encountered. Each day shows two such maxima, but they occur at later times, or smaller sizes on the second day.

CONCLUSIONS

The OST worked as designed. No obvious crosstalk exists between the interior and exterior environment which shows that the closing mechanism worked properly during this experiment. Flushing characteristics are very good, flushing time was about ten minutes in this environment. System accuracy and stability are excellent (about 10 micrograms per liter). Beam attenuations generally decrease and clearly show peaks in the settling velocity distribution. Unresolved is the cause of the low amplitude low frequency fluctuations in the interior of the OST.

Subsequent work on the OST should concentrate on calibration, reduction of data and study of the low frequency fluctuations.

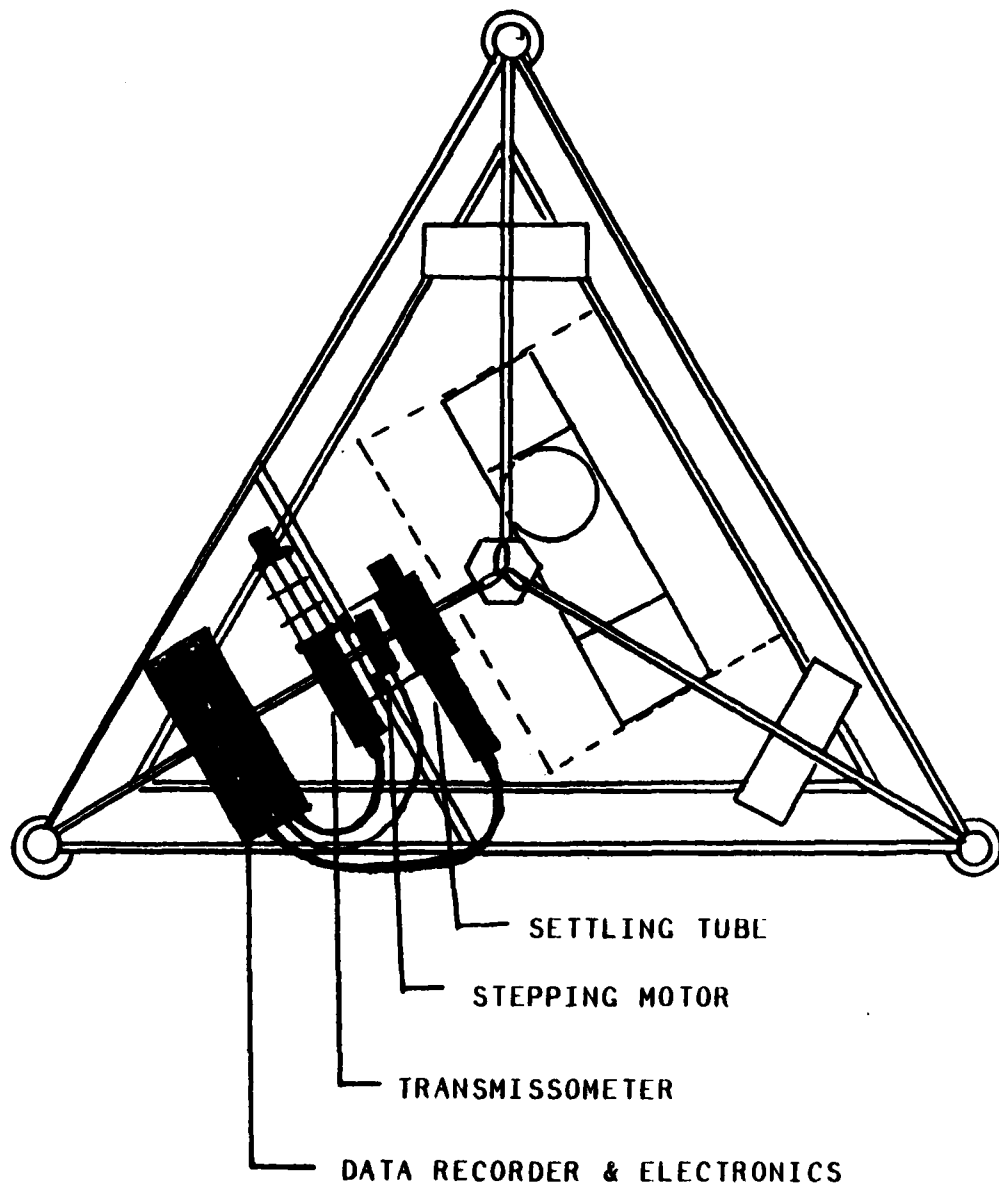


FIGURE 1A

DEEP DEPLOYMENT OF O.S.T. DAY 0

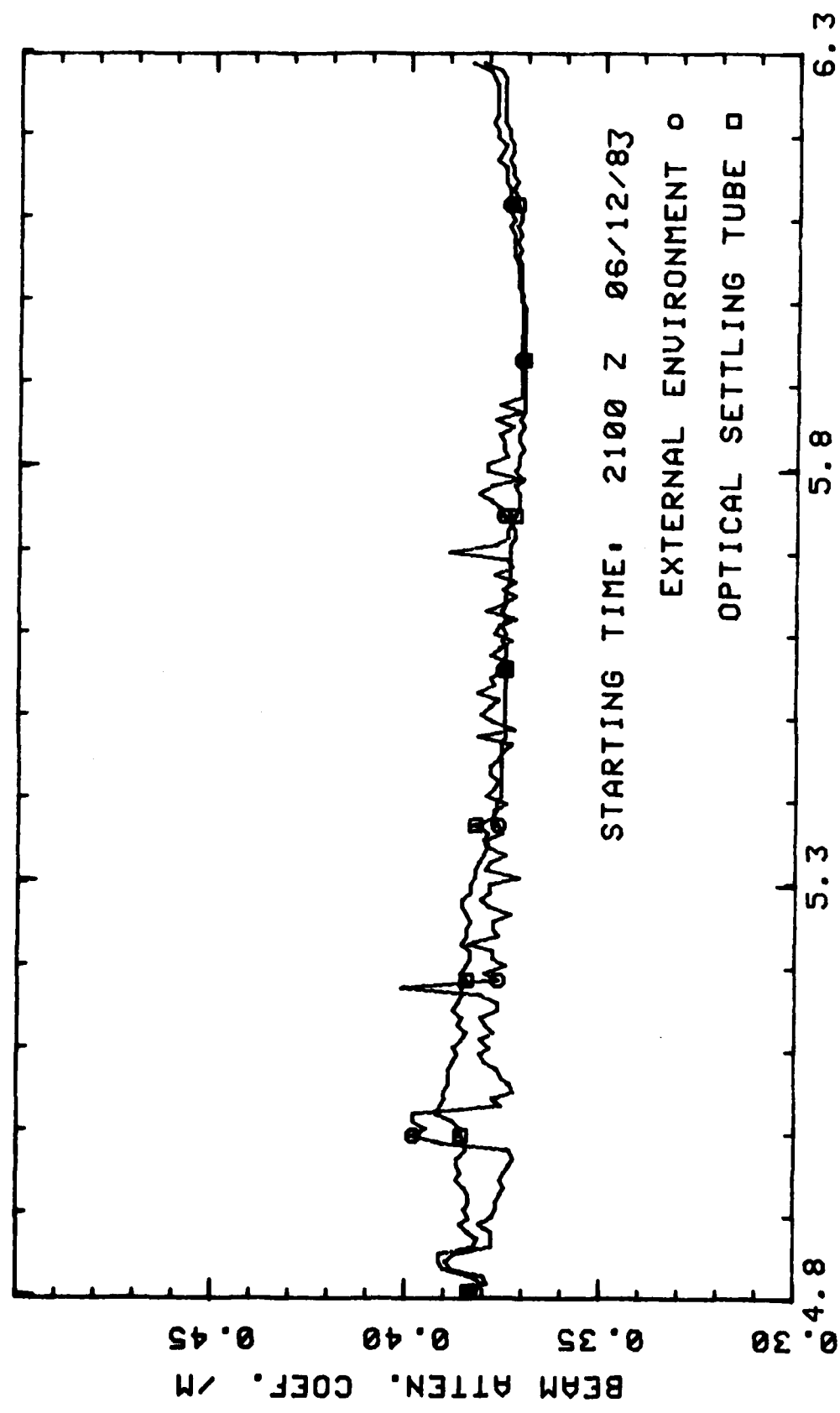


FIGURE 1

DEEP DEPLOYMENT OF O.S.T. DAY 0

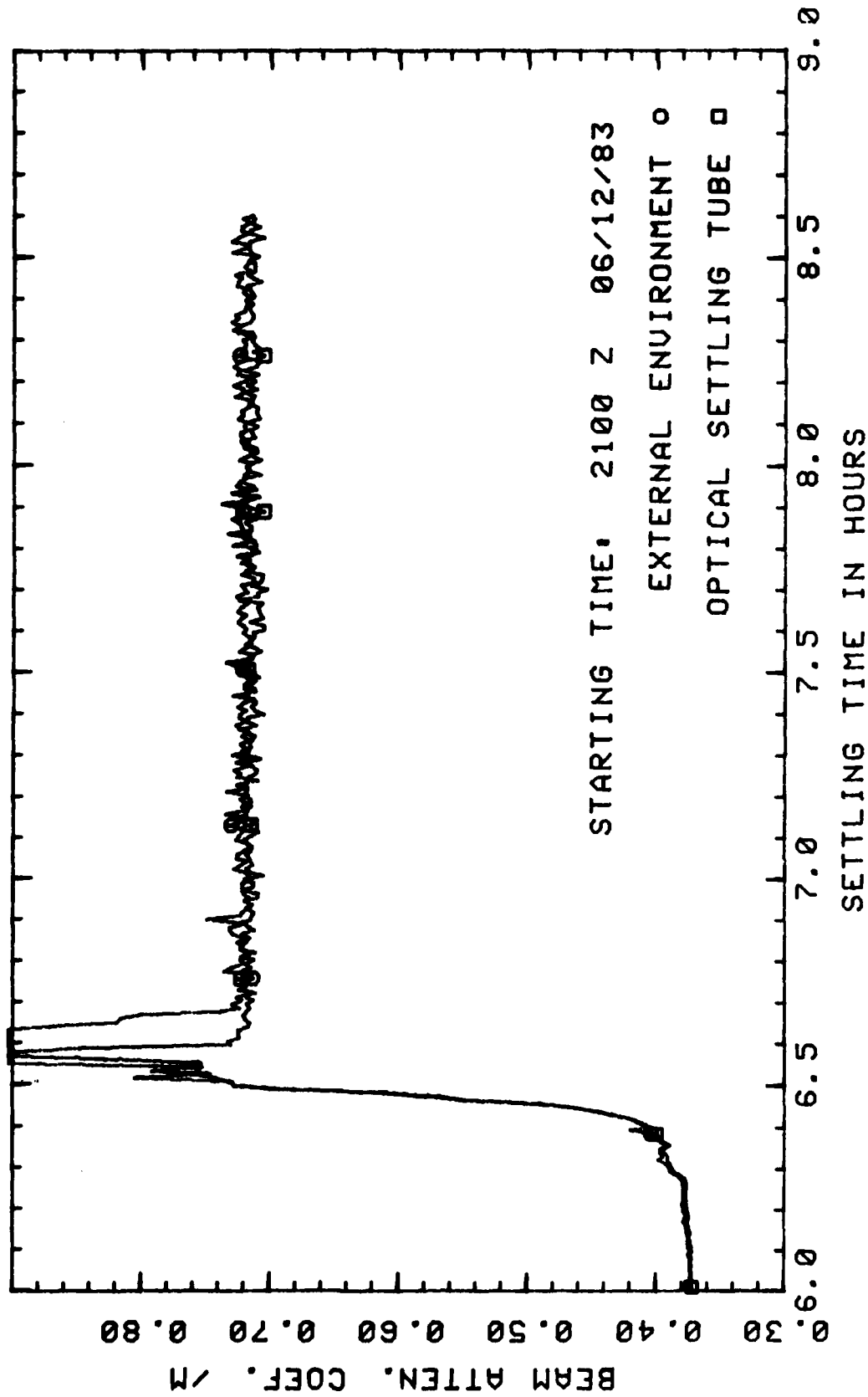
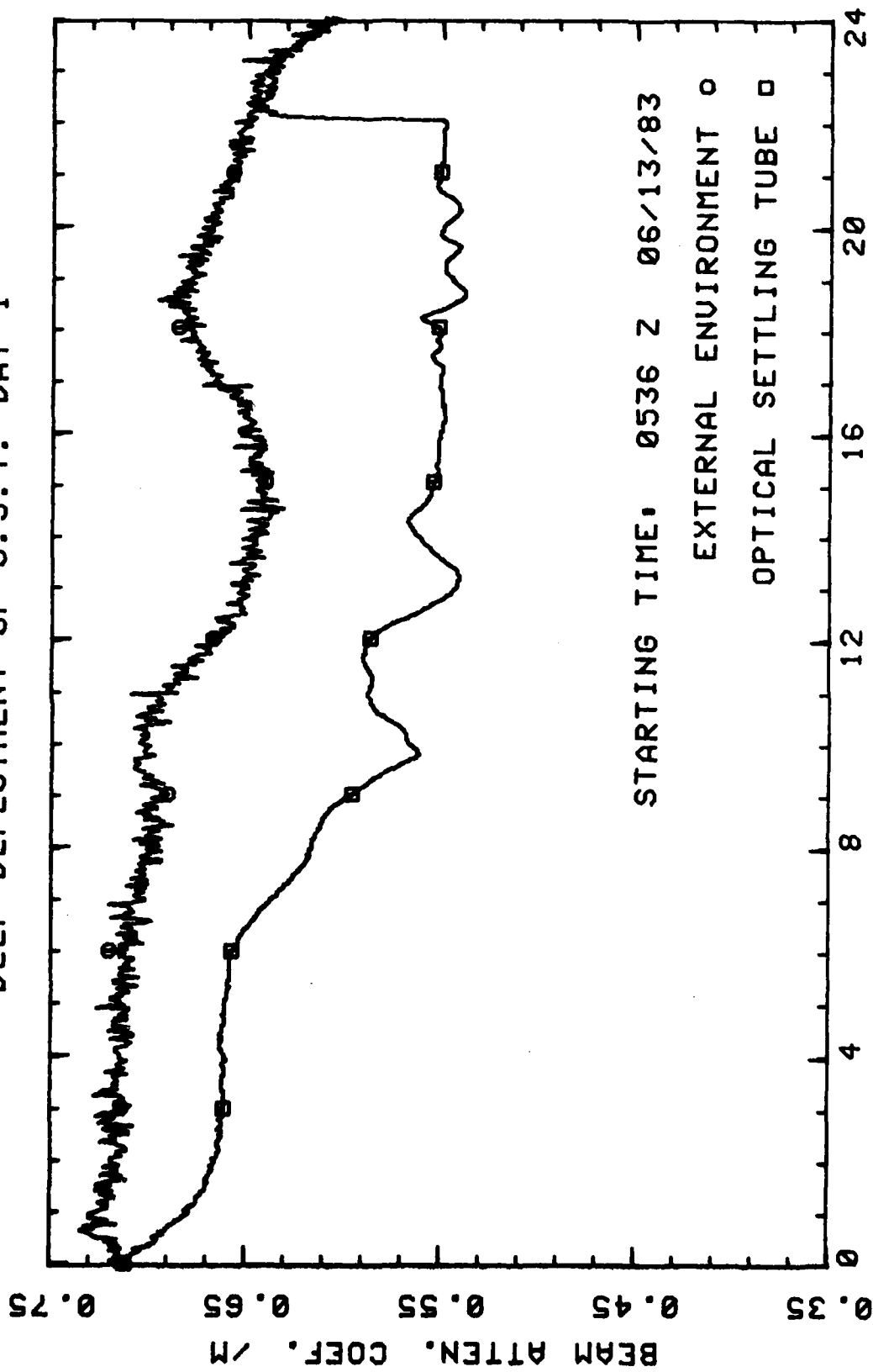


FIGURE 2

DEEP DEPLOYMENT OF O.S.T. DAY 1



STARTING TIME: 0536 Z 06/13/83

EXTERNAL ENVIRONMENT ○

OPTICAL SETTLING TUBE □

SETTLING TIME IN HOURS

FIGURE 3

DEEP DEPLOYMENT OF O.S.T. DAY 1

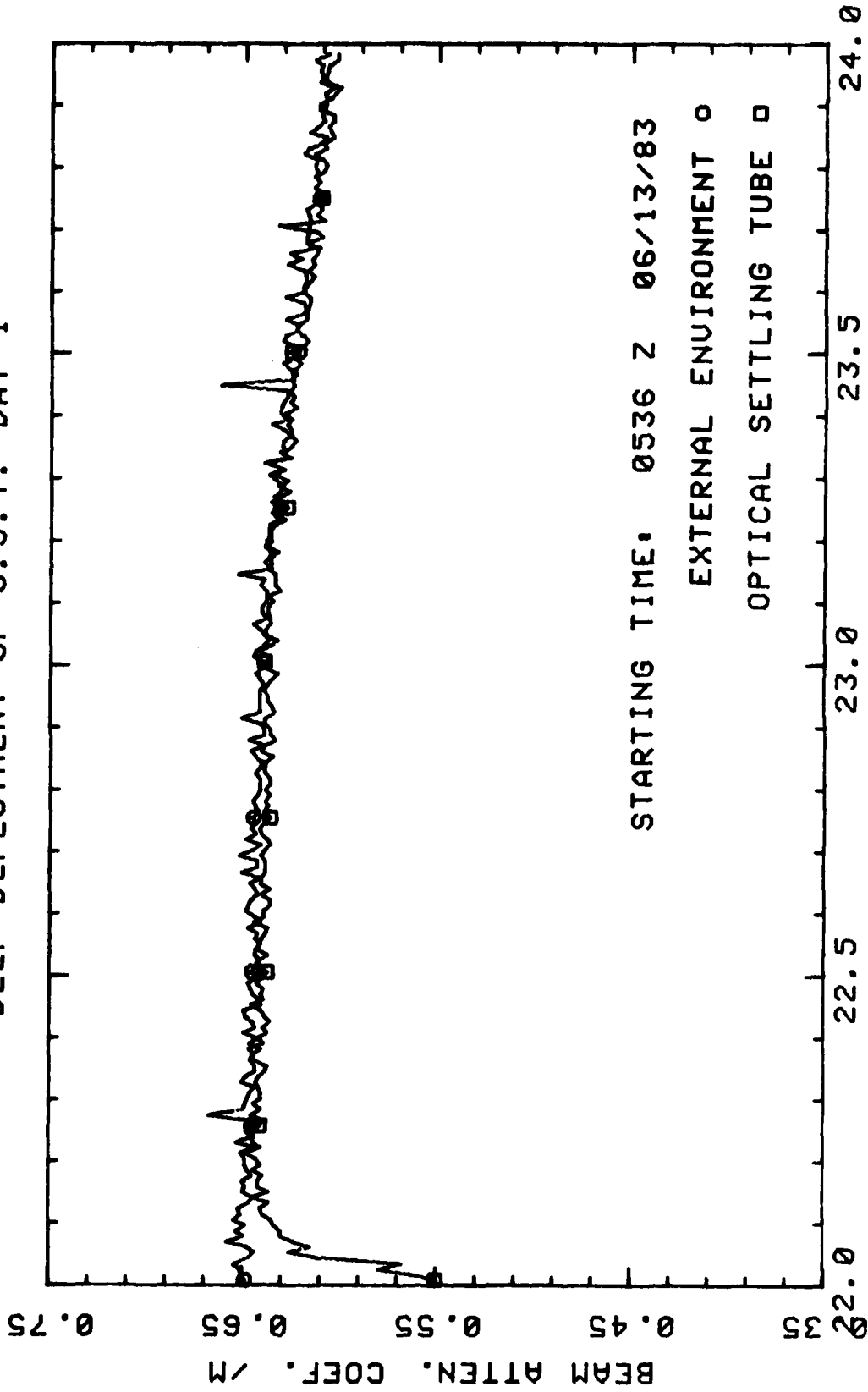


FIGURE 4

DEEP DEPLOYMENT OF O.S.T. DAY 2

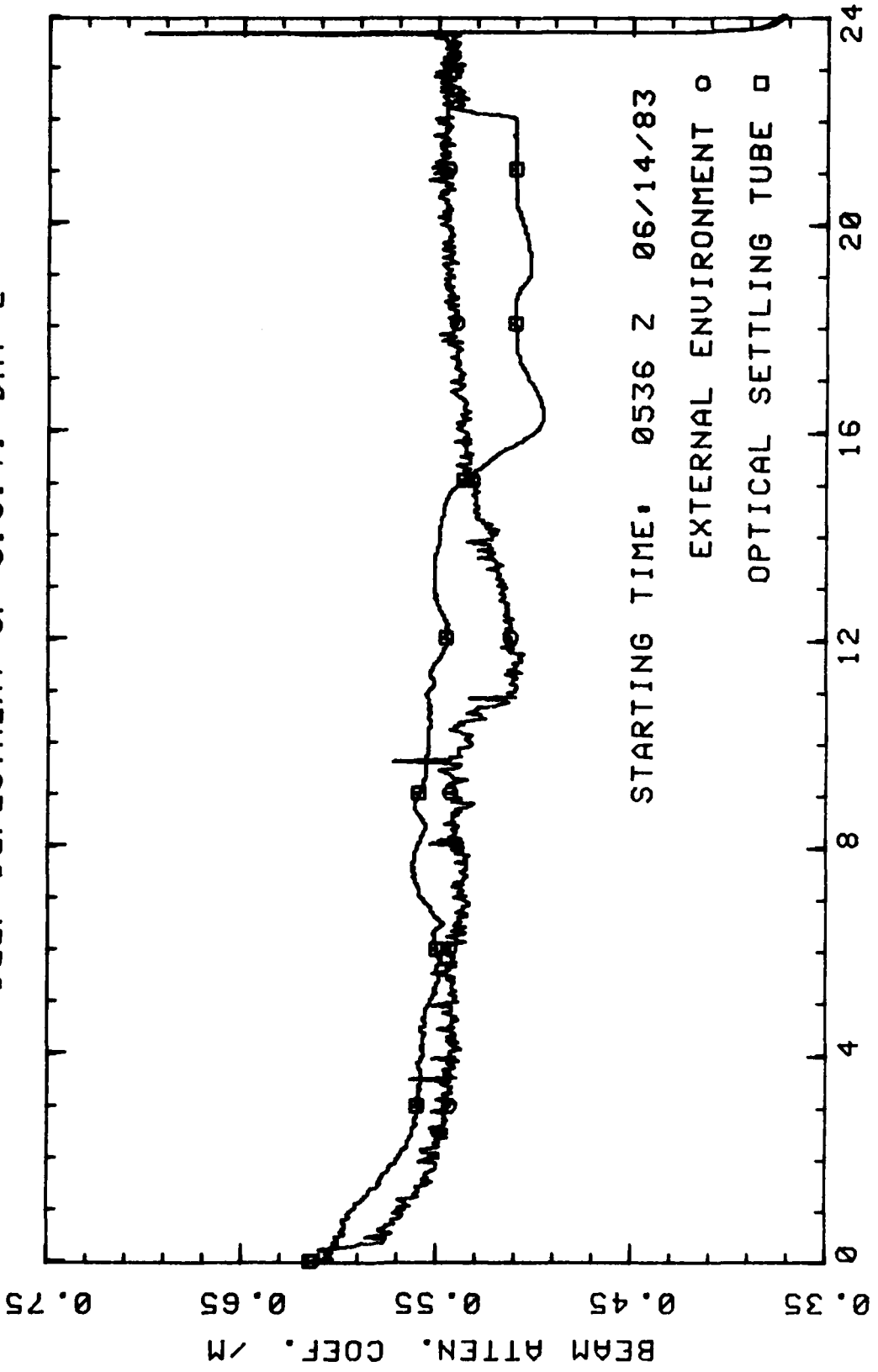
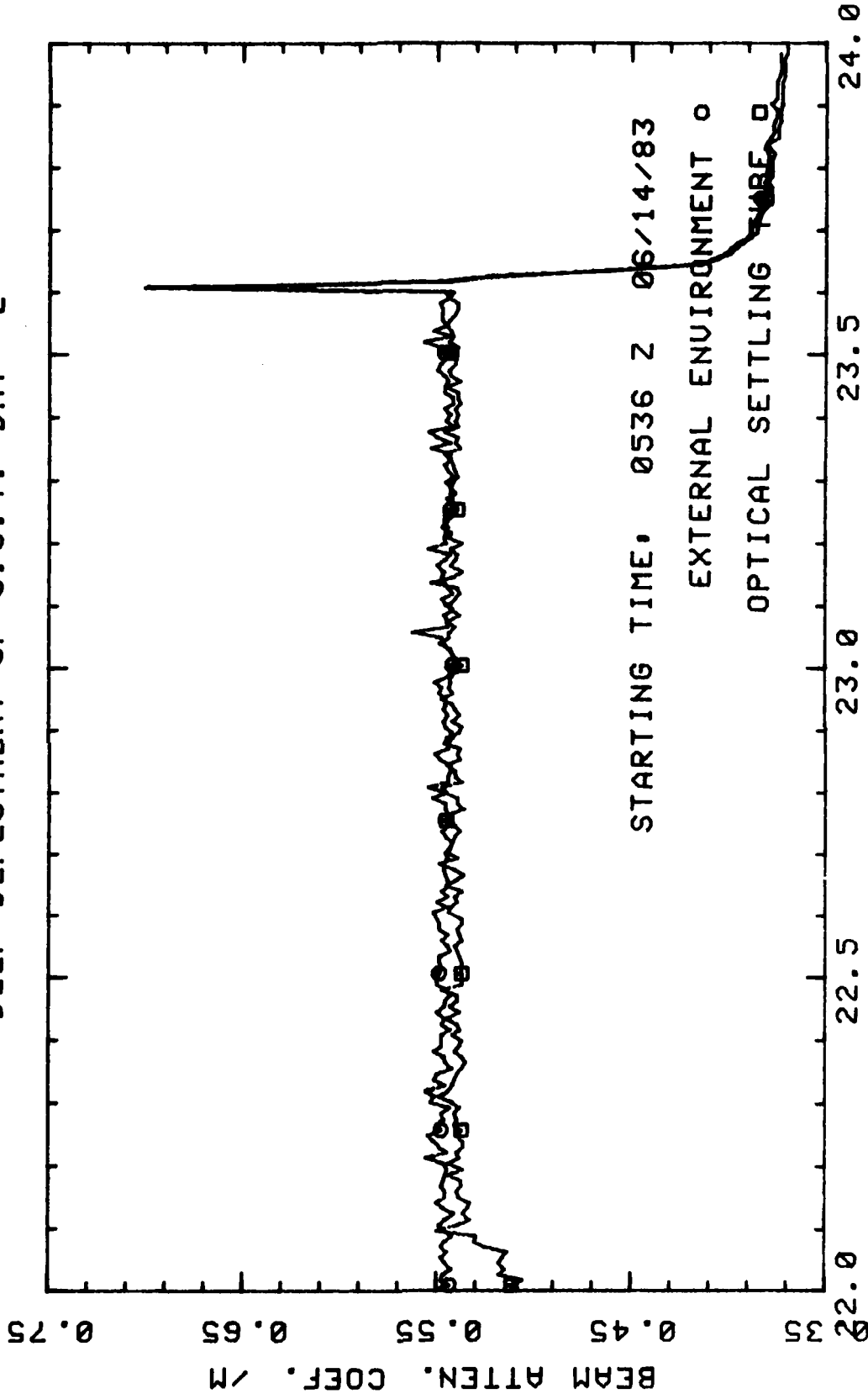


FIGURE 5

DEEP DEPLOYMENT OF O.S.T. DAY 2



SETTLING TIME IN HOURS

FIGURE 6

DEEP DEPLOYMENT OF O.S.T. DAY 2

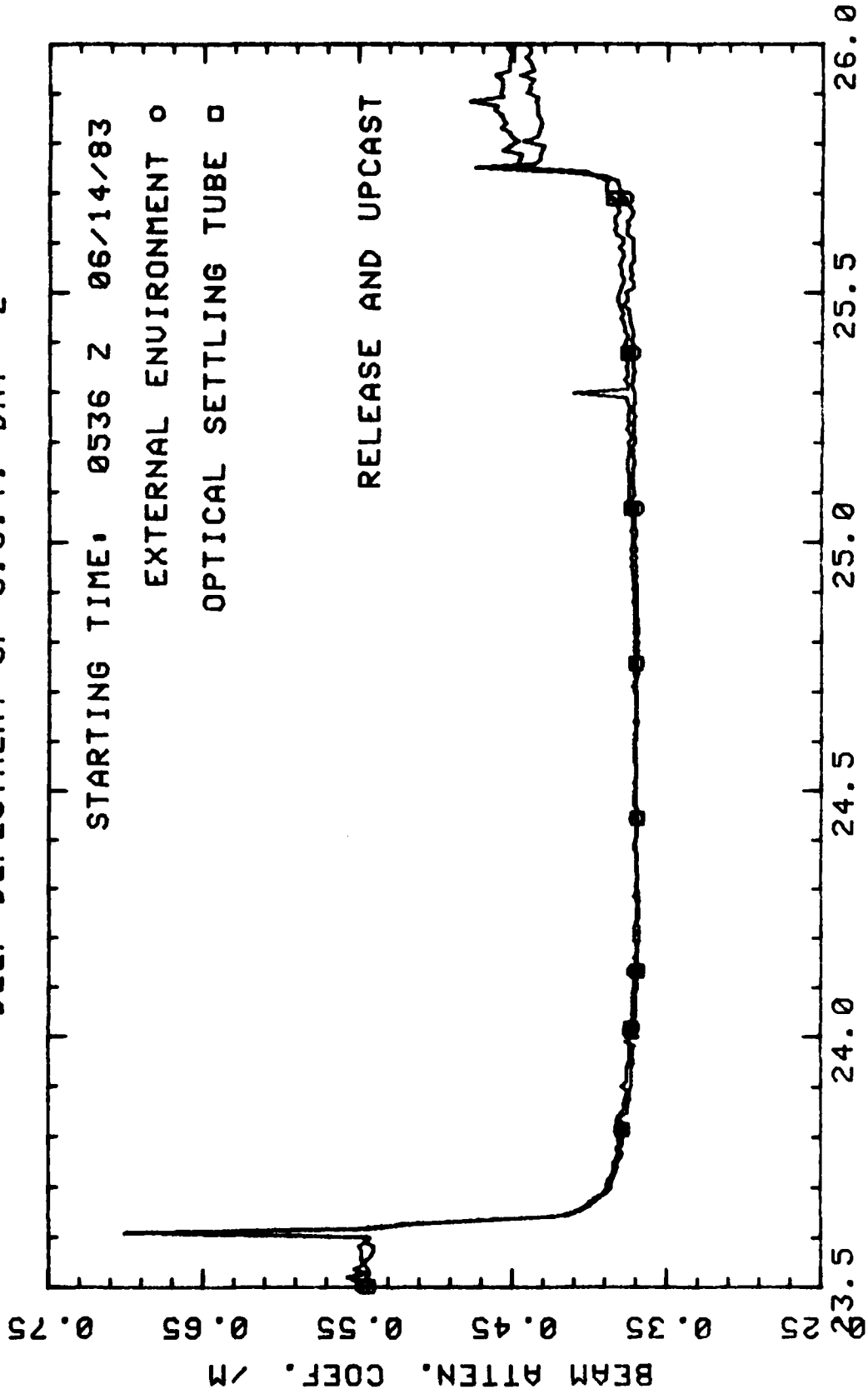


FIGURE 7

DEEP DEPLOYMENT OF O.S.T. DAY 1

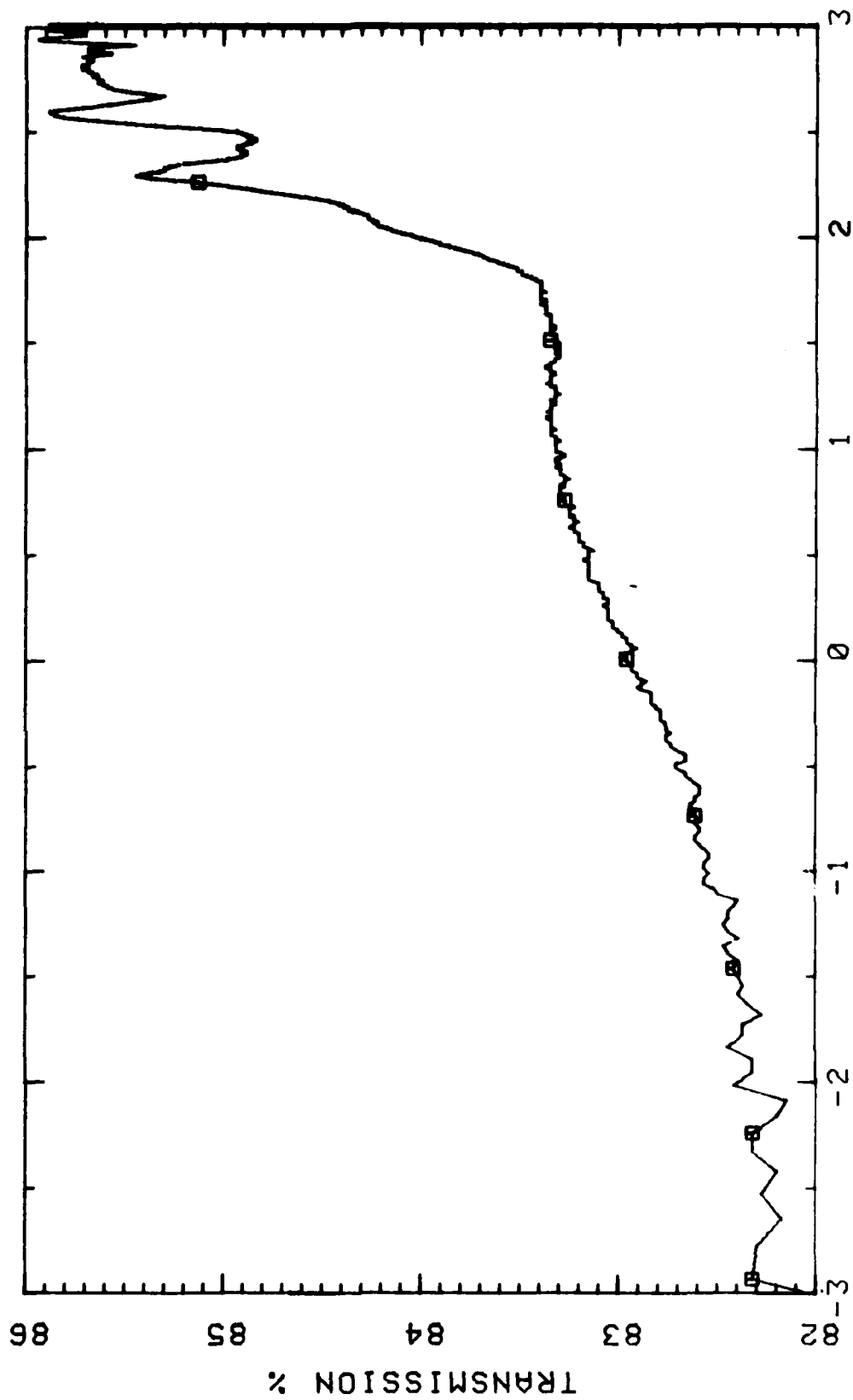


FIGURE 8

DEEP DEPLOYMENT OF O.S.T. DAY 2

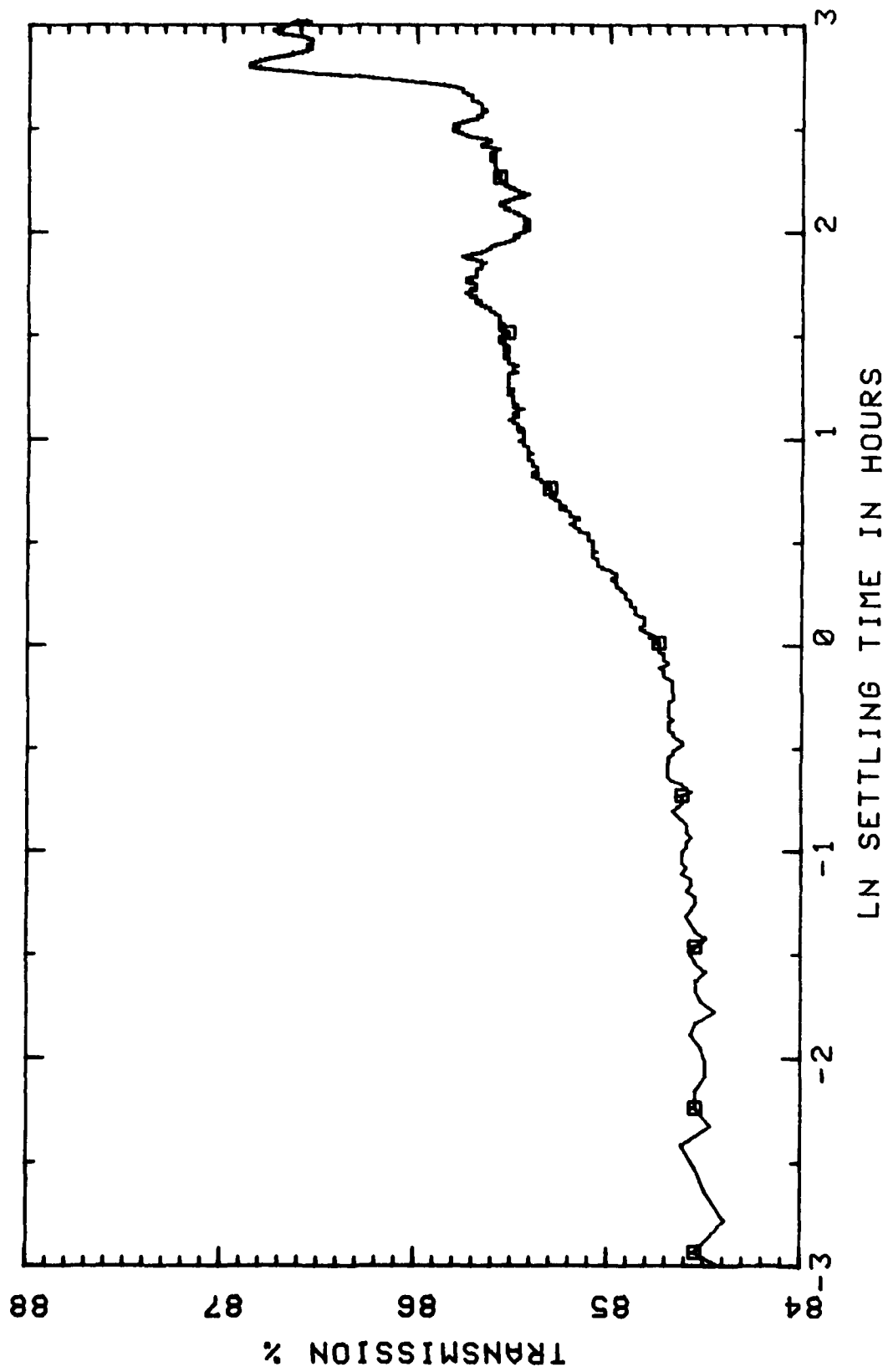


FIGURE 9

APPENDIX 1

AN OPTICAL SETTLING TUBE FOR THE DETERMINATION OF PARTICLE-SIZE DISTRIBUTIONS

J. RONALD V. ZANEVELD, RICHARD W. SPINRAD and ROBERT BARTZ

School of Oceanography, Oregon State University, Corvallis, OR 97331 (U.S.A.)

(Received January 26, 1982; revised and accepted April 20, 1982)

ABSTRACT

Zaneveld, J.R.V., Spinrad, R.W. and Bartz, R., 1982. An optical settling tube for the determination of particle-size distributions. *Mar. Geol.*, 49: 357-376.

The particle-size distribution, the settling-velocity distribution and the concentration-weighted settling velocity are important parameters in the study of sediment dynamics. These parameters can be determined by means of an optical settling tube in which the concentration of particles is determined by means of a beam-attenuation meter and the particle size is determined by Stokes' settling. Results obtained by this method compare very well with Coulter Counter and gravimetric settling tube data. Various correction factors are discussed. The instrument is designed for eventual use in situ.

INTRODUCTION

The determination of the size distribution of suspended particulate matter in the ocean is of considerable interest to researchers studying geological processes. Swift et al. (1972) have given a review of the various methods used to determine particle-size distributions. One method that has not received much attention in the last decade is the so-called photo-extinction method. In this method a well-mixed water sample containing suspended matter is monitored by an optical device as the particles settle. By making use of the relationships between particle size, optical phenomena and settling velocity a size distribution may be deduced. The method has several advantages: the particles can be analyzed without first removing them from the suspending fluid; the sampling method does not disturb the particles; and the method can potentially be used to make in-situ determinations of particle-size distributions, even at great depths in the ocean. It is with the third factor in mind that we have revived the photo-extinction method, using the latest technology in optical oceanography.

Typical results using the photo-extinction method are reported by Rose (1953), Simmons (1959) and McKenzie (1963). Each of these authors showed good results for the photo-extinction method compared with data obtained by microscopic analysis. Burt and Beardsley (1969) have discussed some of the problems associated with the early photo-extinction devices. All

of the authors quoted used simple optical devices with a white light source and employed detectors which were not temperature compensated, although some used constant temperature baths. The use of a white light source leads to problems in assigning the proper optical properties to a particle of a given size, as these properties depend on wavelength. One must furthermore, account for the optical properties of the suspending medium, which is difficult for a polychromatic light source. A monochromatic light source should thus be used. It is further necessary to measure a well-defined optical property so that comparisons with optical properties of particulate matter obtained by theory may be properly applied. The term "extinction" is no longer used since it has not been rigorously defined. Most researchers, in fact, attempted to measure the beam attenuation, which is the attenuation of a perfectly collimated beam of monochromatic light. (For a more exact definition see Jerlov, 1976, and below.) In order to obtain the beam-attenuation coefficient for a collection of particles, the collimation angle must be very small, and the temperature dependence of the detector must be eliminated.

In an earlier publication (Bartz et al., 1978), we have described an in-situ beam transmissometer that uses a nearly monochromatic light source (660 nm wavelength), a high degree of beam collimation (less than 0.8°) and which is temperature compensated (less than 0.1% error in a temperature range of 0° – 25°C). This instrument was incorporated into a settling tube, solving many of the problems of the older instruments. The instrument was interfaced through an A/D converter to a small computer, which regulated the timing of measurements, and which automatically recorded the measurements on a small disk recorder. In this manner we were able to eliminate errors introduced by human observers, and this allowed closer spacing of measurements. We use the rigorous theory derived by Mie (1908) to relate the particle size and index of refraction to beam attenuation. Earlier workers used the approximate relation first obtained by Rose (1953).

THEORY

The beam-attenuation coefficient, c , is defined as the internal attenuation of an infinitesimally thin layer of the medium normal to the beam, divided by the thickness of the layer (Jerlov, 1976). The absorption coefficient, a , and the scattering coefficient, b , are similarly defined. Loss due to attenuation from a well-collimated monochromatic beam of light is due to both light absorption in the beam and scattering away from the beam. Hence,

$$c = a + b \quad (1)$$

The units of a , b and c are m^{-1} .

In natural waters, attenuation is caused by water itself and by suspended and dissolved materials. In an attenuation measurement using natural water all of these must be accounted for, particularly when using white light. In our instrument we use a light emitting diode with a wavelength of 660 nm

for the light source, because in the red region of the spectrum the attenuation due to dissolved materials (the so-called "yellow matter") is negligible (Jerlov, 1976). For natural waters, at 660 nm wavelength we thus have:

$$c = c_{\text{water}} + c_{\text{particles}} \quad (2)$$

In practice, the beam-attenuation coefficient is obtained by means of a transmission measurement. The transmission of a collimated beam along a light path of length r , $T(r)$, is given by:

$$T(r) = \exp(-cr) \quad (3)$$

and hence:

$$c = -\frac{1}{r} \ln T(r) \quad (4)$$

In order to interpret the observed beam-attenuation coefficients, it is necessary to know the relationship between the beam-attenuation coefficient and the properties of the particles, the size and index of refraction. In order to do this we can make use of the theory derived by Mie (1908) which describes the perturbation of a plane monochromatic wave by a dielectric sphere.

There is some question as to whether the theory, which gives the distribution of scattered light for a single particle, can be applied to a collection of particles. Van de Hulst (1957) indicates that if the particles are separated by 3 times the radius, the distance is sufficiently large to insure independent scattering. In an example he cites particles of 1 mm diameter. For much smaller particles, with diameters of 2.89 μm , Woodward (1964) indicates that multiple scattering is negligible for volume concentrations less than 2×10^{-4} or about 400 mg l^{-1} . Woodward (1964) states that Napper and Ottewill observed that multiple scattering started when particles were separated by 50 times their diameter.

The criteria listed above are readily met by a 25 mg l^{-1} suspension of 100- μm diameter particles. Oceanic particle suspensions rarely exceed concentrations of 1 mg l^{-1} , and the great majority of particles in the ocean are less than 10 μm in diameter. One may thus conclude that for the great majority of particle suspensions in the ocean, the particles scatter independently and multiple scattering is not likely to be a problem.

The instrument described is primarily designed to be used for eventual application to in-situ measurements in the deep ocean, so that loosely aggregated organic matter will not be a significant part of the particle ensemble. In the discussions that follow, we will therefore assume that the particulate matter will not contain significant amounts of loosely aggregated particles or organic matter other than skeletal materials.

Mie's (1908) theory gives the total scattered and absorbed radiation by a particle, I , from a randomly polarized beam of light. When this quantity I is divided by the cross-sectional area $\pi D^2/4$ of the particle one obtains the attenuation efficiency factor $K(D)$ (also known as the effective area coeffi-

cient). It then follows that for $N(D)$ particles with diameter D per unit volume, the attenuation coefficient for particles, c_p , can be defined as:

$$c_p = K(D) N(D) \frac{\pi D^2}{4} \quad (5)$$

For the case of a polydisperse system, with lower and upper size limits D_1 and D_2 , respectively, the attenuation coefficient is given by:

$$c_p = \frac{\pi}{4} \int_{D_1}^{D_2} K(D) N(D) D^2 dD \quad (6a)$$

which can be approximated by:

$$c_p = \frac{\pi}{4} \sum_{D_i} K_i N_i D_i^2 \Delta D \quad (6b)$$

where the subscript i refers to the i th size component.

In general, the index of refraction is given by $m = n - in'$, where n is the real and n' is the imaginary part of the index of refraction ($n' = a\lambda/4\pi$, where a is the bulk absorption coefficient of the particles). Van de Hulst (1957) has obtained a limiting expression for the attenuation efficiency when the complex index of refraction is close to unity, $|m - 1| \ll 1$. The requirement that $|m - 1| \ll 1$ means that both $n - 1$ and n' have to be $\ll 1$, which is typically the case in oceanic suspensions. For quartz $n = 1.2$ for example, and $n' < 0.1$ for organic matter.

The expression for the attenuation efficiency obtained by Van de Hulst (1957) is given by:

$$K(D) = 2 - 4 \exp(-\rho \tan \beta) \frac{\cos \beta}{\rho} \sin(\rho - \beta) - 4 \exp(-\rho \tan \beta) \left(\frac{\cos \beta}{\rho}\right)^2 \cos(\rho - 2\beta) + 4 \left(\frac{\cos \beta}{\rho}\right)^2 \cos 2\beta, \text{ where:} \quad (7)$$

$$\beta = \tan^{-1} \left(\frac{n'}{n - 1} \right) \text{ and:}$$

$$\rho = \frac{2\pi D}{\lambda} |n - 1|$$

λ is properly defined as the wavelength of light in the medium, so that in

applying eq. 7 we must set $\lambda = \frac{\lambda_{\text{vacuum}}}{m_{\text{water}}}$, and similarly $m = \frac{m_{\text{particles}}}{m_{\text{water}}}$.

A relation for the absorption efficiency of a particle is also given by Van de Hulst (1957):

$$K_{\text{absorption}} = 1 + \frac{2\exp(-4xn')}{4xn'} + \frac{2\exp(-4xn') - 2}{(4xn')^2} \quad (8)$$

where $x = \pi D/\lambda$. Figure 1 shows the attenuation and absorption efficiencies for various parameters. It is seen that for large diameters (and hence large ρ and x), the attenuation efficiency approaches 2 and the absorption efficiency approaches 1. This is because a large sphere will absorb all the light that strikes it, while it diffracts the same amount of light it intercepts (Babinet's principle). If we assume that the suspended matter has a relative index of refraction of 1.2 (which is close for quartz, calcite, kaolinite and montmorillonite, among others), one can calculate that the attenuation-efficiency factor stays within 10% of 2 for spherical particles larger than $7 \mu\text{m}$ in diameter, independent of absorption properties. Only for spherical particles of less than $7 \mu\text{m}$ diameter, for aggregates, or for suspensions with large amounts of organic matter, will it be necessary to apply eq. 7 to obtain the attenuation efficiency.

If $n' = 0$ (non-absorbing particles) eq. 7 reduces to:

$$K_{\text{attenuation}} = 2 - \frac{4}{\rho} \sin \rho + \frac{4}{\rho^2} (1 - \cos \rho) \quad (9)$$

Equation 9 can be used for suspended materials of non-biological origin, as their absorption is very small.

Using eq. 7 or 9 together with eq. 6a or 6b we can relate the number of particles of a given size to their attenuation. Next, we need to determine the attenuation due to particles in a size range. This is accomplished by monitoring the beam attenuation as a function of time at a known distance from the top of a tube as the particles settle. By means of Stokes' equation for the settling rate of small particles (and assuming spherical particles), we can assign a particle-size range for each time interval. The change in beam attenuation in the same time interval can then be ascribed to the particles in that size range.

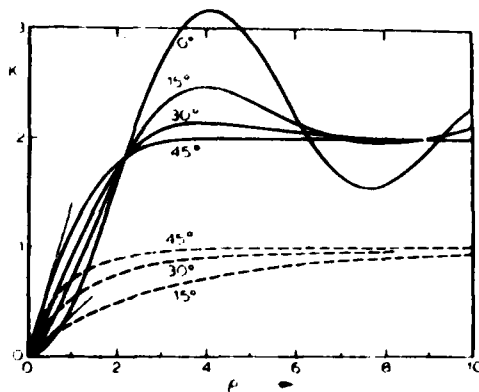


Fig. 1. The attenuation and absorption efficiencies as functions of $\rho = 2\pi D(m-1)/\lambda$. The angle indicated on the figure is $\tan^{-1} n'/(n-1)$ where n' is the imaginary part of the index of refraction and n is the real part. For a particle with a relative index of refraction 1.2 and $\lambda = 660 \text{ nm}$, $D = 0.52 \rho$.

The Stokes' equation for the settling velocity of particles is given by:

$$W_s(D) = \frac{1}{18} \frac{(d_s - d) g D^2}{\nu} \quad (10)$$

where d_s is the density of the particle, d is the density of the suspending fluid, g is the acceleration due to gravity, and ν is the viscosity of the fluid. Stokes' equation is valid when the Reynold's number is less than 0.5 (Prandtl and Tietjens, 1957), which is certainly the case for particles with diameters less than 100 μm settling in water. A particle settling a distance h in time t ($W_s = h/t$) has a diameter given by:

$$D = \left[\frac{18 h \nu}{(d_s - d) g t} \right]^{1/2} \quad (11)$$

In time interval $\Delta t = t_1 - t_2$, particles with diameters between D_1 and D_2 obtained by substitution of t_1 and t_2 , respectively, into eq.11, will have settled out of the water column. The beam attenuation due to particles with sizes between D_1 and D_2 , $c_p(D_1, D_2)$, is equal to the difference in beam attenuation measured at corresponding times t_1 and t_2 , $c(t_1) - c(t_2)$. By use of eq.6a we then deduce that:

$$c(t_1) - c(t_2) = c_p(D_1, D_2) = \frac{\pi}{4} \int_{D_2}^{D_1} N(D) D^2 K(D) dD \quad (12)$$

where D_1 and D_2 are obtained by substituting the times of observation into eq.11. If we choose D_1 and D_2 to be close, we can approximate eq.12 by:

$$c_p(D_1, D_2) = \frac{\pi}{4} N_p(D_1, D_2) D_*^2 K(D_*) \quad (13)$$

where $N_p(D_1, D_2)$ is the number of particles between diameters D_1 and D_2 per unit volume and D_* is a value between D_1 and D_2 . Typically the mean value is chosen for D_* , which introduces a very small error, as $D_1 - D_2$ in our observations ranges from 0.5 μm for sand-size particles to 0.005 μm for clay-size particles.

Solving eq.13 for the number of particles between D_1 and D_2 yields:

$$N_p(D_1, D_2) = \frac{4c_p(D_1, D_2)}{\pi D_*^2 K(D_*)} \quad (14)$$

where D_* is obtained from eq.11 and $K(D_*)$ is obtained from eq.7 or 9, and $c_p(D_1, D_2)$ is a measured quantity.

PRESENTATION OF DATA

There are several ways of presenting particle-size distributions. One way is a size histogram, which is obtained by plotting results from eq.14 directly. More common are the cumulative and differential particle-size distributions. The cumulative particle-size distribution, $p(D)$, is defined as the number of

particles per unit volume with diameters larger than D . The differential particle-size distribution, $f(D)$, is defined as the number of particles per unit volume with sizes between D and $D + dD$. The relationship between the two is then given by:

$$p(D) = \int_D^{\infty} f(D') dD', \text{ or} \quad (15)$$

$$f(D) = \frac{d}{dD} p(D) \quad (16)$$

For a very small range of D , we may approximate eq. 16 by:

$$f(D_*) = \frac{p(D_1) - p(D_2)}{|D_1 - D_2|} \quad (17)$$

where D_* lies between D_1 and D_2 . From the definition of the cumulative size distribution it follows that:

$$p(D_2) - p(D_1) = N_p(D_1, D_2) \quad (18)$$

so that

$$f(D_*) = \frac{N_p(D_1, D_2)}{|D_1 - D_2|} \quad (19)$$

From eqs. 19 and 14 it is thus possible to calculate the differential size distribution. We have chosen to display our results as a differential size distribution, because it shows maxima and minima as a function of size much more clearly than a cumulative size distribution and is, therefore, a more critical test of the instrument.

METHODS

A schematic presentation of the optical settling tube system is shown in Fig. 2. Figure 3 shows a more detailed picture of the settling tube. Output of the transmissometer is in the form of 0–5 V (D.C.), corresponding to 0–100% transmission. The data are processed by the analog-to-digital converter and immediately stored in the buffer of the Apple II minicomputer. Upon completion of a settling measurement (which may take as long as the operator chooses) the data are stored under a named data file on a diskette. Processing programs may then be run through the computer and the data manipulated as desired.

The electronic design and characteristics of the circuitry within the beam transmissometer are described by Bartz et al. (1978). This reference describes a transmissometer having an optical pathlength of 0.25 m but the pathlength in the settling tube is 0.05 m. This represents the only significant difference between the transmissometer in use here and the one referred to.

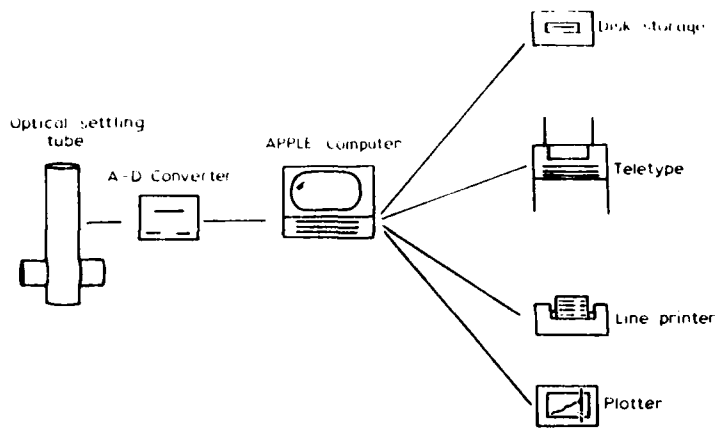


Fig.2. Diagram of the optical settling-tube system.

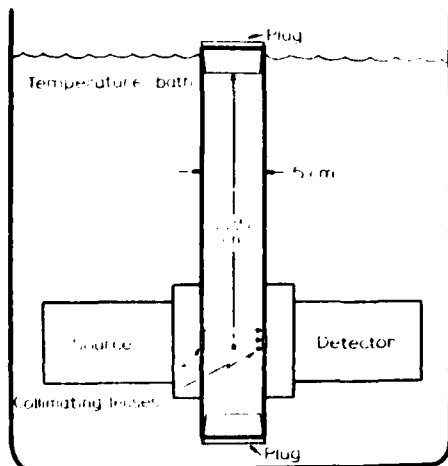


Fig.3. The optical settling tube.

The temperature bath surrounding the settling tube is used to minimize fluctuations in temperature, and hence, viscosity, of the settling medium. Viscosity plays an important role in the equation of Stokes settling velocity, so it is essential to keep the viscosity changes to a minimum.

An experiment is performed by mixing a particle sample with the water in the settling tube to obtain a homogeneous suspension. The computer is then supplied with the necessary input to begin receiving data. This input is the number of observations to be made, the time interval between observations, the index of refraction and the density of the particles. The maximum number of observations is 250 total, however no maximum exists in the time interval between observations. This enables detection of an extremely large range of particle sizes. Upon completion of the experiment the data are

placed on a disk file. The original plot of transmission versus time can then be transcribed onto the platter and the size-frequency distribution may also be plotted or printed out on the teletype or line-printer.

The method of data acquisition involves the use of a constant time interval between transmission observations. Using a constant time scale results in a change of the diameter interval between observations. However, this is corrected for by means of eq.19. It is possible to program a varying time interval between observations as the settling progresses, but we have not found this necessary.

In addition to calculating and plotting the particle-size distribution as outlined above, the existing computational scheme allows for the determination of a concentration-weighted settling velocity for each sample. This single value arises from the consideration that the total mass flux due to particle settling must be equal to the summation of the mass fluxes for each integral size component within the overall distribution. Thus when the equation of mass conservation for the total size distribution is equated with a similar expression for the sum of the components, the single-valued concentration-weighted settling velocity can be shown to be:

$$W_s = \frac{\sum_{i=1}^n P_i W_{si}}{\sum_{i=1}^n P_i} \quad (20)$$

(J.D. Smith, pers. commun., 1981)

where P_i = the mass concentration of size component i , and W_{si} = the settling velocity of size component i .

Physically, this term represents the ratio of the mass flux to mass concentration and thus provides a parameter by which to identify the particle size distribution. A unique correlation has been shown to exist between the concentration-weighted settling velocity and the slope of the hyperbolic particle size distribution characteristic of oceanic particulates (Peterson, 1977).

RESULTS

Four different suspensions were chosen to test the performance of the optical settling tube: aluminum spheres, latex spheres, an ocean mud sample and quartz. The first two samples were obtained from a supply house (Particle Information Services, Inc.) which provides well-defined, ideal particles for instrument calibration, and the latter two samples came from natural oceanic sediments.

The aluminum spheres are sieved and processed at the factory to remove irregularly shaped particles. Ninety-six percent of the particles, by number, according to the supplier's specification, used in this experiment fall between

sieves number 200 (American Society of Testing Materials) and number 230, corresponding to diameters of 74 and 62 μm , respectively. The density of the aluminum is 2.7 g cm^{-3} and the refractive index used is approximately 1.22 relative to water.

The latex particles are composed of polystyrene divinyl benzene resin with a mean diameter of 70 μm and a standard deviation of less than 7 μm . The latex spheres represent more of a monodisperse particle-size distribution than any other sample used in this experiment. These particles have a density of 1.06 g cm^{-3} and a relative refractive index of 1.20. These particles are sized at the factory using an "air classifier" which appears to be a centrifugal sizing device.

The mud sample was obtained during a research cruise in 1972 off the Oregon coast. The location of the sample was 46° 0.1'N 124° 58.2'W, in the Astoria Canyon at a depth of 1491 m. The sample is an olive mud and based on previous geologic studies of the Astoria Canyon (Russell, 1967; Carlson, 1968) it is known that the clays of this area are dominated by montmorillonite, with illite and chlorite present in smaller amounts. A density of 2.7 g cm^{-3} and a relative index of refraction of 1.2 were used for the sample.

The quartz sample was treated with 10% HF (5 min), 6N HCl (15 min) and 2N NaOH (60 min) to remove the organic carbonate components as well as disaggregate the sample. Settling and decantation were used to obtain a particle-size range of 3–10 μm . Quartz has a density of 2.65 g cm^{-3} and a relative refractive index of 1.2.

Figure 4 shows the time rate of change of transmission for each of the four samples. While the time axis is labeled 0–100 in each case, the actual duration of the measurement varied from 250 s in the case of the aluminum spheres to 20,000 s for the mud sample. The duration of the measurement can be varied to include the size range of interest. The transmission axis is absolute and identical in all four experiments. Transmission values covered the full range of the instrument: from nearly 0% to the clean water value of 98%. Also demonstrated in Fig. 4 is the behavior of each of the types of particle-size distributions. Starting with the monodisperse latex spheres the sudden jump in transmission at roughly 1500 s (time = 60) corresponds to a large number of particles settling out of the beam. The aluminum spheres are nearly monodisperse, and thus they, too, demonstrate the sudden jump in transmission (bearing in mind that the time scale for the aluminum spheres is one-tenth that of the latex spheres). The mud sample, which was chosen as being more representative of the type of suspension to be found in the natural environment, demonstrates the gradual changes in transmission characteristic of a polydisperse size distribution. The shape of the curve for the mud indicates the experiment could have been run for an even longer time period to obtain information about the fine clay particles within the sample. The quartz sample shows a gradual increase in transmission followed by a leveling-off indicative of a well-defined particle size distribution. The same sample was also tested in a gravimetric settling tube and the Coulter Counter.

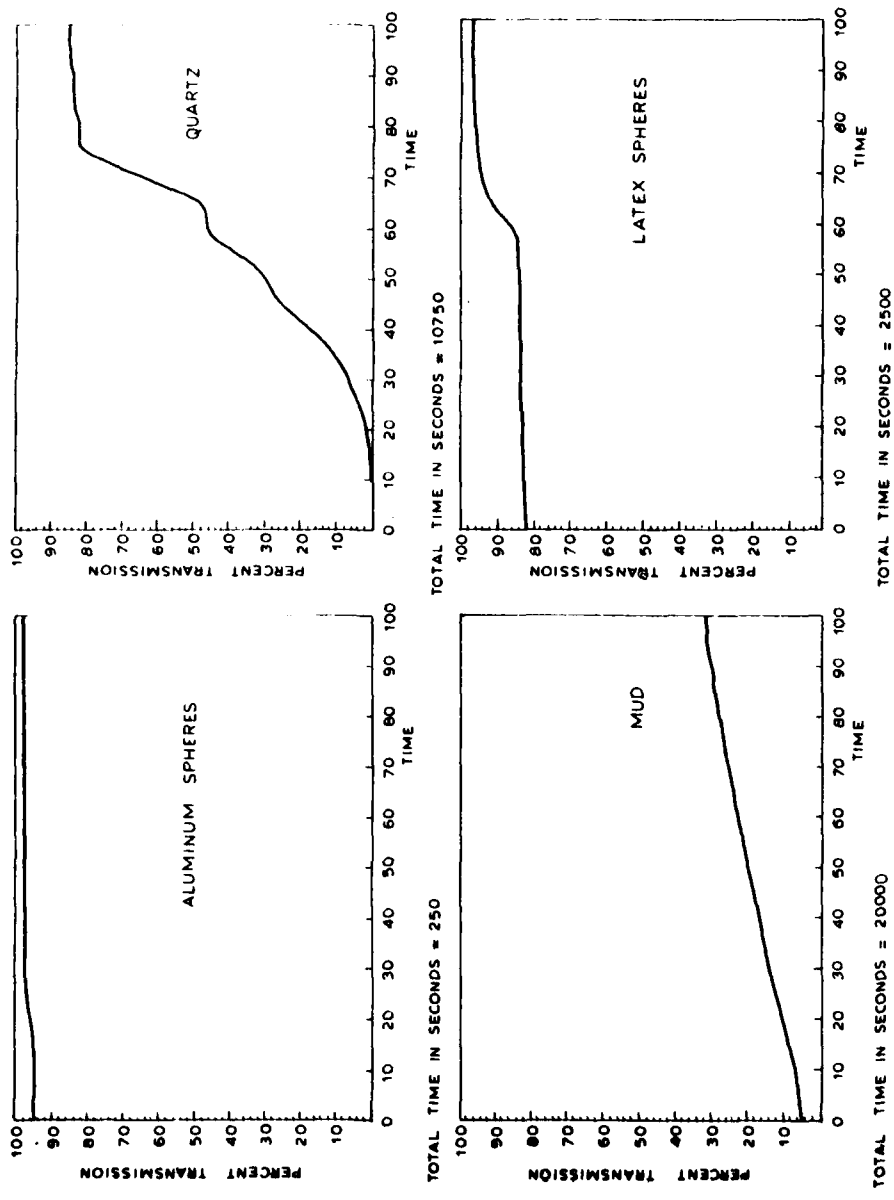
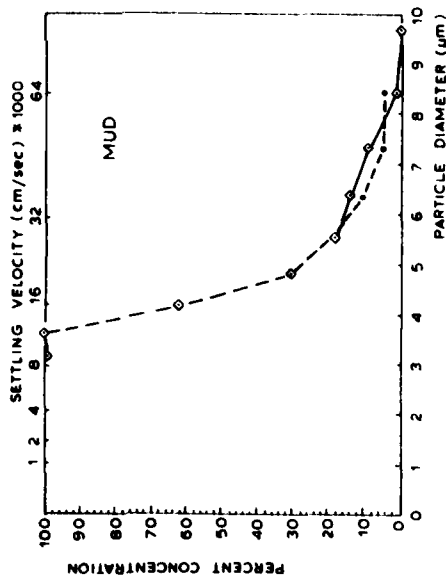
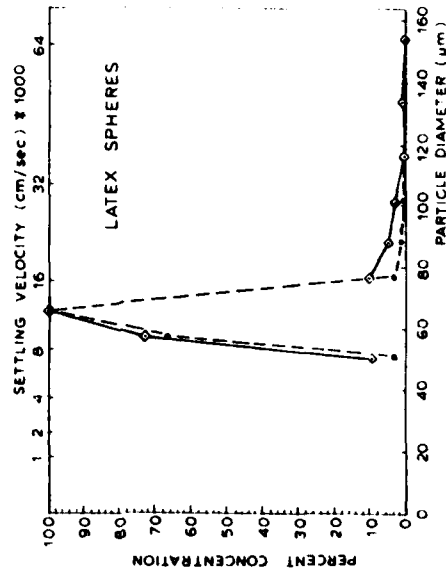
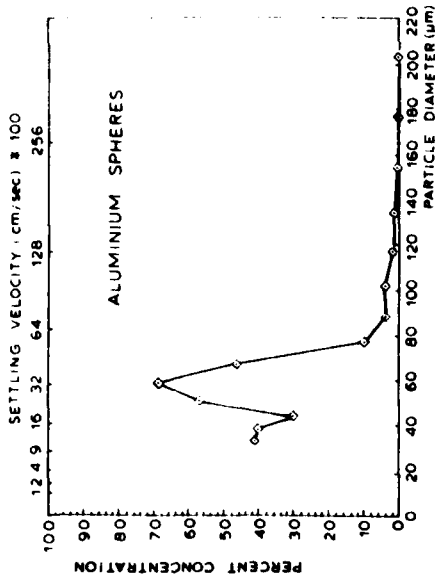
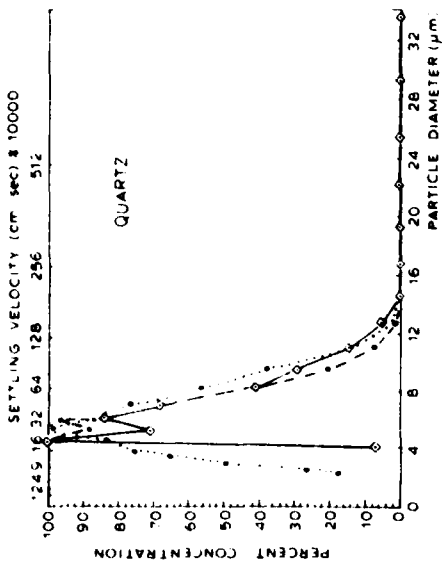


Fig. 4. Time series of transmission for various materials as they settle in the optical settling tube. The time scale is relative, with total time indicated beneath each graph. The transmission scale is absolute.



CONCENTRATION-WEIGHTED SETTLING VELOCITY (cm/sec) = 0.298327497

CONCENTRATION-WEIGHTED SETTLING VELOCITY (cm/sec) = 0.0801900071

Figure 5 shows relative differential particle-size distributions as obtained from the optical settling tube, the Coulter Counter and, in the case of quartz, the gravimetric settling tube. The results indicate good agreement among the instruments. For the quartz particles the gravimetric settling tube gave a mean particle diameter of $6.8 \mu\text{m}$ ($\phi = 7.2$) and a standard deviation of $5.0 \mu\text{m}$; similarly, the optical settling tube yielded a mean value of $7.7 \mu\text{m}$ ($\phi = 7.0$) and a standard deviation of $4.7 \mu\text{m}$; the Coulter Counter gave results of $6.3 \mu\text{m}$ ($\phi = 7.3$) and $5.0 \mu\text{m}$ for the mean and standard deviation, respectively. The mud sample gave nearly identical results for the Coulter Counter and the optical settling tube. In fact the mean difference in particle concentration as a function of size is only 3.7% between the two instruments.

The size distributions of the latex spheres also demonstrated good agreement between the optical settling tube and the Coulter Counter. In this case the mean values of the particle-size distribution are $69.2 \mu\text{m}$ ($\phi = 3.85$) for the Coulter Counter and $70.7 \mu\text{m}$ ($\phi = 3.82$) for the optical settling tube. Corresponding standard deviations are 16.6 and $13.6 \mu\text{m}$.

The aluminum spheres could not be analyzed with the Coulter Counter due to the low electrical resistivity of aluminum. The Coulter Counter is calibrated for particles having a much higher resistance than aluminum. However, information from the supplier indicates that the particle size should be between 60 and $75 \mu\text{m}$. Indeed the results obtained indicate a mean diameter of $74.1 \mu\text{m}$ ($\phi = 3.75$) and a peak diameter of $70.1 \mu\text{m}$ ($\phi = 3.83$). This implies skewing toward the large end. This may have been caused by aggregation or flocculation of the particles within the settling tube, or by inclusion of forward-scattered light (see below for a discussion). In fact, for the aluminum spheres some problems with flocculation were experienced during the introduction of the particles into the settling tube.

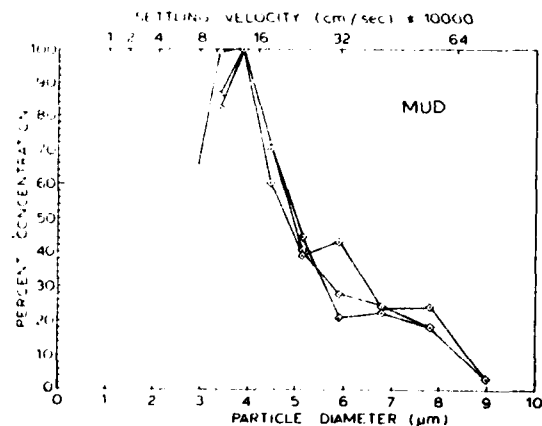


Fig. 6. Size distributions obtained by repeated analysis of the same sample.

Fig. 5. Differential particle-size distributions obtained by means of the optical settling tube (solid lines), Coulter Counter (dashed lines), and gravimetric settling tube (dotted lines).

In order to check the repeatability of the instrument we repeated the measurement of the mud sample three times. Results are shown on Fig.6.

DISCUSSION

By using a nearly monochromatic light source and a temperature-compensated detector, as well as a constant temperature bath, we have overcome the objections to the photo-extinction method raised by Burt and Beardsley (1969). Figure 5 shows that the particle-size distributions obtained with the optical settling tube are nearly the same as those obtained by means of a Coulter Counter and a gravimetric settling tube. In fact, differences between size distributions obtained with the various devices are similar to differences from repeated observations of the same material with the optical settling tube (Fig.6). This is even more remarkable when we consider that the optical settling tube measures particle attenuation and settling velocity, the Coulter Counter measures electrical resistivity of particles, and the gravimetric settling tube measures weight and settling velocity. Particle attenuation is proportional to the cross-sectional area of the particle, whereas resistivity and weight are proportional to the volume of the particle. Since the surface to volume ratio increases as particle size decreases for a given volume of particles, the optical device might then appear to be relatively less sensitive to the larger particles depending on other factors. It is therefore of interest to study the theoretical limits of the sensitivity of the optical settling tube to particle concentration.

Using eq.5, we can write the following equation for the minimum detectable change in beam attenuation, Δc_{\min} , as a function of the minimum number of particles detectable per unit volume, N_{\min} , and diameter, D_i :

$$\Delta c_{\min} = N_{\min} \frac{\pi D_i^2}{4} K_i \quad (21)$$

The beam transmissometer is accurate to 0.1% over a temperature range of 0–25°C. At a constant temperature, however, the accuracy is 0.02%. The smallest change in beam attenuation occurs when the transmission is large. We will thus find Δc_{\min} at the pure-water value of 98% transmission. Using eq.4 for $T = 98.00\%$ and $T = 97.98\%$ we find that $\Delta c_{\min} = 0.405 \text{ cm}^{-1}$ for a pathlength of 5 cm. We can now use eq.21 to find the corresponding minimum-detectable particle-number concentration, N_{\min} (units cm^{-3}). We used $K = 2$ for convenience in this calculation. Table I shows the results of this calculation, both for a 5-cm path and a 100-cm path, to which we will refer later. From the minimum-detectable number concentration we obtained the minimum-detectable weight concentration by multiplying by the particle volume and density. We used a density of 2 g cm^{-3} in our calculations. Results are shown in Table I.

It is clear from Table I that the optical settling tube-beam attenuation meter becomes less sensitive to weight concentration as the particle size increases, but becomes more sensitive to the number concentration. At first glance a minimum detectable weight concentration of $270 \mu\text{g l}^{-1}$ for

TABLE I

The minimum-detectable number concentration N_{\min} (cm^{-3}) for light paths of 5 and 100 cm, and the minimum-detectable weight concentration conc_{\min} ($\mu\text{g l}^{-1}$) for light paths of 5 and 100 cm. The calculations were made for a minimum-detectable transmission change of 0.02%, an attenuation efficiency factor of 2, a specific gravity of 2 gm cm^{-3} and a beam diameter of 1.5 cm

D (μm)	N_{\min} 5 cm (cm^{-3})	N_{\min} 100 cm (cm^{-3})	Conc_{\min} 5 cm ($\mu\text{g l}^{-1}$)	Conc_{\min} 100 cm ($\mu\text{g l}^{-1}$)
100	0.26	0.021	270.2	22.0
50	1.03	0.084	135.1	11.0
20	6.45	0.525	54.0	4.40
10	25.8	2.10	27.0	2.20
5	103	8.40	13.5	1.10
2	645	52.5	5.40	0.44

the 100- μm particles might seem inadequate, but this represents only one particle for every four cm^3 . This concentration thus is lower than can statistically be handled in a meaningful way by routine Coulter Counter procedures in which only a few cubic centimeters of fluid are counted. The optical settling tube has a detection volume of 8.84 cm^3 (beam diameter = 1.5 cm and beam length = 5 cm), which is larger than the volume typically counted in a Coulter Counter analysis. The minimum detectable concentration for 100- μm particles would correspond to about two particles in the detection volume. It is concluded that for 100- μm particles, the optical settling tube is almost capable of counting individual particles and therefore for sizes over 100- μm is as sensitive as a Coulter Counter. As the particle size decreases the minimum-detectable weight concentration decreases proportional to $1/D$ and is more than adequate for laboratory work.

The device was designed for eventual application to in-situ determination of particle-size distributions. In that case the minimum concentrations of Table I are larger than would be encountered in the cleanest ocean waters. This problem can be solved by using a greater pathlength. We also calculated the minimum-detectable number and weight concentrations for a 100-cm path (see Table I). This pathlength would allow us to detect concentrations of a few $\mu\text{g l}^{-1}$ for particles less than 20 μm diameter. Above that size, the instrument would be capable of detecting individual particles, and therefore would be at least equivalent in accuracy to a Coulter Counter.

A second potential problem is the determination of the attenuation efficiency of the suspended particles. As we have shown in eq.7, the two parameters that determine the attenuation efficiency are ρ and β . For $m = 1.20$, which includes most of the minerals found in the ocean, the attenuation efficiency, K , lies within 10% of 2.0 for $D > 7.5 \mu\text{m}$; for sizes smaller than that, we must use eqs.7 or 9. For particulate matter with indices of refraction lower than 1.20, K does not approach 2 as fast. Oceanic materials

with low indices of refraction tend to be organic in nature however, and therefore have complex indices of refraction, with relatively large values for β . This tends to dampen the oscillations of K about 2 for the smaller diameters. Figure 1 shows for example, that particles with relative indices of $m = 1.02 - 0.1i$ ($\beta = 45^\circ$) have K -values almost exactly equal to 2 for $D \geq 8 \mu\text{m}$. One is thus probably safe in using $K = 2$ for all oceanic particles with $D \geq 8 \mu\text{m}$, so that good results can be expected even when the nature of the material is unknown. For particles smaller than $8 \mu\text{m}$, the nature of the material must be known if K is to be determined accurately. This constitutes a potential limitation of the in-situ use of optical settling tubes in those near-bottom regions where biological activity is high, but should present no problems in the deep ocean.

A final problem which deserves attention is the error introduced by the inclusion of near-forward scattered light in the detected beam. The collimation angle, Θ , of the beam attenuation meter used with the experiment was $\Theta = 0.75^\circ$. We can set:

$$c_{\text{theo}} = c_{\text{observed}} + 2\pi \int_0^\Theta \beta(\Theta) \sin\Theta d\Theta \quad (22)$$

Using eq.5 we can rewrite eq.22 for a single particle as follows:

$$\frac{\pi D^2}{4} K_{\text{theo}} = \frac{\pi D^2}{4} K_{\text{obs}} + \beta_f, \quad (23)$$

and hence:

$$K_{\text{obs}} = K_{\text{theo}} \left(1 - \frac{\beta_f}{c_{\text{theo}}} \right) \quad (24)$$

The uncorrected beam-attenuation coefficient is thus always underestimated and K_{theo} , the theoretical value of the attenuation efficiency, is always larger than K_{obs} , the value one would use in eq.5 to obtain the actual beam-attenuation coefficient. The error in K is not constant as the percentage of light that is scattered into the near-forward direction increases as the particle size increases and as the relative index of refraction decreases.

Using the scattering tables of Shifrin and Salganik (1973), we calculated the ratio of β_f/c_{theo} as an indication of the error for the quartz and mud samples. In the case of the quartz sample the ratio is 0.032, and in the case of the mud sample the ratio is 0.012. For diameters less than $8 \mu\text{m}$ the error is thus a few percent and can be ignored.

For larger particles, the forward-scattered light can be a significant part of the attenuation. For example, a $30\text{-}\mu\text{m}$ particle with a relative index of refraction of 1.15 scatters into a cone of one degree 55% of all the light it scatters.

The forward scattered light makes the attenuation-efficiency factor, K , appear to be less than 2. Much theoretical (see Brillouin, 1949) and experimental work (Rose, 1952) has been carried out in order to explain the

observed attenuation by means of a reduced K . The reduction in K depends on both the collimation angle and particle size. Mie (1908) theory allows one to calculate the correction term in eq.22, so that the empirical approach of Rose (1952) is in principle not necessary. The series solution of Mie converges very slowly for large particles however, so that tables for the calculation of the error factor in attenuation measurements do not exist for particles larger than 30 μm . It should be noted that for narrow size distributions such as the latex spheres sample of Fig.5, K_{obs} is nearly constant over the relatively narrow size range, so that it will not affect the relative particle-size distribution, which is thus correct.

In order to obtain an accurate size distribution over a large size range of particles, such as would be the case for in-situ measurements, the effect of the curve obtained by Rose (1952) is not generally valid since it applies to a collimation angle of 1° and was obtained for silica sand. Rose's assertion that K_{obs} approaches unity for large spheres is correct only for absorbing materials. In that case, the total attenuation approaches the "geometrical shadow" in the limit. This can be seen from Fig.1. For large spheres nearly all scattered light is directed into the forward direction, and hence K_{obs} approaches K_{theo} which approaches 1. For very large non-absorbing spheres K_{theo} is 0, so that for large sizes K_{obs} also approaches 0.

Approximate expressions for the light scattering by large particles have been derived by Van de Hulst (1957). The expressions are valid if $\pi D/\lambda \gg 1$ and $\pi D|m - 1|/\lambda \gg 1$, which is the case for inorganic materials, but not for living cell tissue. Combining his expressions for the diffracted light and the refracted light gives:

$$i_1(\Theta) + i_2(\Theta) = \frac{2\chi^2 J_1^2(\chi \sin\Theta)}{\sin^2\Theta} + \frac{8\mu^2 \chi^2}{(4\mu^2 + \Theta^2)^2} \quad (25)$$

where $i_1(\Theta) + i_2(\Theta)$ is the intensity distribution of light scattered by a particle with parameters $\chi = \pi D/\lambda$; $\mu = m - 1$. $J_1(z)$ is the first order Bessel function. $J_1(z)$ can be approximated by expressions given in the Handbook of Mathematical Functions (1966). We used eq.25 to correct for the near-

TABLE II

The ratio of light scattered into the cone between $\Theta = 0^\circ$ and 0.75° and the total scattering coefficient for large particles. Calculations were made for a relative index of refraction of 1.20. Results were identical to three significant places for a relative index of refraction of 1.15

Particle diameter (μm)	β_t/b
30	0.382
50	0.419
70	0.448
90	0.452
110	0.461

forward scattering of large particles. Table II shows the fraction of all the scattered light that is scattered into a cone of 0.75° as a function of size and index of refraction. It is seen that the index of refraction has a negligible influence as the scattered light is dominated by diffracted light.

CONCLUSIONS

It was found that accurate particle-size distributions can be obtained by means of an optical settling tube with a beam-attenuation meter as the optical device. The light source has to be nearly monochromatic with a wavelength in the red region, in order to reduce attenuation by dissolved materials to a minimum. The nearly monochromatic light source allows one to accurately relate the observed beam attenuation to concentration if the particle size is known. Equations allowing the calculation of correction factors for the relative index of refraction of the particles and the near-forward scattered light included in the attenuation measurement were derived. As beam attenuation meters have been used extensively in the deep ocean, the optical settling tube concept can be applied to measurements of non-aggregated, inorganic particle-size distributions in the deep ocean.

ACKNOWLEDGEMENT

This work was supported by the Office of Naval Research through contract N00014-79-C-0004, as part of the High Energy Benthic Boundary Layer Experiment.

We thank Dana Wimer for typing the manuscript.

REFERENCES

- Abramowitz, M. and Stegun, I.A., 1966. Handbook of Mathematical Functions. U.S. Dept. of Commerce, National Bureau of Standards, pp.369-370.
- Bartz, R., Zaneveld, J.R.V. and Pak, H., 1978. A transmissometer for profiling and moored observations in water. Soc. Photo-Optical Instrumentation Eng., "Ocean Optics V", pp.102-108.
- Brillouin, L., 1949. The scattering cross section of spheres for electromagnetic waves. J. Appl. Phys., 20: 1110-1125.
- Burt, W.V. and Beardsley Jr., G.F., 1969. Underwater optical measurements. Oceanology Int., 4: 5-39.
- Carlson, P.R., 1968. Marine Geology of Astoria Submarine Canyon. Ph.D. Thesis, Oregon State University, Corvallis, Oreg., 259 pp.
- Jerlov, N.G., 1976. Marine Optics. Elsevier, Amsterdam, 231 pp.
- McKenzie, K.G., 1963. The adaption of a colorimeter for measuring silt-sized particles - a rapid photo-extinction (PE) method. J. Sediment. Petrol., 33: 41-48.
- Mie, G., 1908. Beiträge zur Optik trüber Medien, speziell kolloidalen Metallösungen. Ann. Phys., 25: 377-445.
- Peterson, R.L., 1977. A Study of Suspended Particulate Matter: Arctic Ocean and Northern Oregon Continental Shelf. Ph.D. Thesis, Oregon State University, Corvallis, Oreg., 122 pp.
- Prandtl, L. and Tietjens, O.G., 1957. Applied Hydro and Aerodynamics. Dover, New York, N.Y., 270 pp.

- Rose, H.E., 1952. Determination of the "Extinction coefficient" - particle size relationship for spherical bodies. *J. Appl. Chem.*, 2: 80-88.
- Rose, H.E., 1953. *The Measurement of Particle Size in Very Fine Powders*. Constable, London, 127 pp.
- Russeli, K.L., 1967. *Clay Mineral Origins and Distribution on Astoria Fan*. M.S. Thesis, Oregon State University, Corvallis, Oreg., 40 pp.
- Shifrin, K.S. and Salganik, I.N., 1973. *Tables for Light Scattering*. Gidrometeoizdat, Leningrad (in Russian).
- Simmons, G., 1959. The photo-extinction method for the measurement of silt-sized particles. *J. Sediment. Petrol.*, 29: 233-245.
- Swift, D.J.P., Schubel, J.R. and Sheldon, R.W., 1972. Size analysis of fine-grained suspended sediments; a review. *J. Sediment. Petrol.*, 42: 122-134.
- Van de Hulst, H.C., 1957. *Light Scattering by Small Particles*. Wiley, New York, N.Y., 470 pp.
- Woodward, D.H., 1964. Multiple light scattering by spherical dielectric particles. *J. Opt. Soc. Am.*, 54: 1325-1331.

APPENDIX 2

A TRANSMISSOMETER FOR PROFILING AND MOORED OBSERVATIONS IN WATER

Robert Bartz, J. Ronald V. Zaneveld and Hasong Pak
School of Oceanography, Oregon State University, Corvallis, Oregon 97331

Abstract

Numerous applications exist for a beam transmissometer that is low in cost, relatively stable, and consumes very little power. In this paper we present the design and calibration of a beam transmissometer that is constructed with P.V.C. to simplify the design and minimize costs, contains stable temperature compensated electronics, and consumes less than 150 milliwatts of power. Accuracy and stability with proper calibration and careful use will provide data with an error of less than 0.5% transmission.

Introduction

The optical oceanography group at Oregon State University has developed a beam transmissometer with a 25 cm light path for profiling and moored observations in water. There are numerous applications for a small, portable meter that can accurately measure profiles of beam transmission and the concentration of suspended matter in relatively turbid natural waters. In working with biological features (1) and geological features (2) it is furthermore clear that the time dependence of the concentration of biological and lithogenic suspensions needs to be known in order to form predictive models of suspensoid dynamics. It is thus important that the instrument be capable of being moored over long time periods.

The instrument measures beam transmission, a well-defined optical parameter, so that the theoretical relationship between particle parameters (size, shape, and index of refraction) and the optical parameter via Mie's theory (3) is straightforward. The instrument is designed for maximum repeatability and minimum power requirements.

In order to appropriately study suspensoid dynamics it is necessary to set out a large number of transmissometers in a vertical and horizontal array. The number of units available on a given budget limits the size of the array and can adversely influence the scientific results of an experiment. Cost was thus an important consideration in the design of the transmissometer.

Transmissometer Design

The light intensity in a well-collimated beam of light decreases exponentially as given by

$$I(r) = I(0) e^{-cr}, \quad (1)$$

where $I(r)$ is the light intensity at distance r from the source and c is the beam attenuation coefficient. If $cr = 1$, the light intensity will have decreased by $1/e$ when it is measured. A beam transmissometer tends to be most accurate in the region where c is on the order of $1/r$, since in this region cr is not too close to zero and on the other hand the signal is also large enough that one is not trying to measure very low light intensities. Since the instrument is designed for relatively shallow depths (300 meters maximum), r was set at 25 cm, giving optimum performance within one and a half orders of $c = 4 \text{ m}^{-1}$.

The light source is a Light Emitting Diode (LED) with a wavelength of 660 nm. This wavelength choice was generated by our desire to eliminate attenuation due to dissolved humic acids (the so-called "yellow matter"). The yellow matter absorbs light strongly at the shorter wavelengths but this effect can be ignored for wavelengths larger than 600 nm.

The transmissometer's mechanical design is shown in Figure 1. The pressure housing has a 300 meter depth capability and is constructed from standard P.V.C. tubing to minimize costs and eliminate problems with corrosion. A collimated light source and optical receiver are located 25 cm apart and are connected by three stainless steel threaded rods. Optical alignment is accomplished by adjusting the length of each connecting rod. Two light stops are placed between the receiver and light source to prevent receiver saturation by direct sunlight entering the receiver. Input power and output signals are fed through a multi-pin marine connector located at the top of the pressure housing. The P.V.C. surfaces adjacent to the light path are painted with anti-fouling paint to prevent blocking of the light path by marine growth.

Optical design of the collimated light source is very simple; the lens used is both the pressure window and collimating element. The planoconvex lens (diameter = 22.4 mm, focal length = 40 mm) is installed so that the flat side is in contact with the water. A LED and



Fig. 1. 25 cm transmissometer.

a temperature sensing diode are potted into a threaded assembly so that the LED can be positioned at the lens focal point in order to collimate the light source. Electro-optical characteristics of the LED, MV5020 are: lens color, clear; lens radius, 2 mm; peak wavelength, 660 nm; spectral line half width, 20 nm; half power point, 45° ; and apparent area (circular), $0.828 \times 10^{-3} \text{ cm}^2$. The resultant light source beam parameters are: beam diameter, 20 mm; beam divergence, 0.5° ; and radiated output power, 3×10^{-7} watt.

The optical receiver consists of a lens having identical characteristics to the one used in the light source with a silicon photovoltaic detector located at the focal point. The detector is potted into a threaded assembly to enable alignment of the detector. The detector used is an EG&G PV100A and has the following characteristics: active area, 5.1 mm^2 ; spectral range, 350 - 1150 nm; and responsivity at 660 nm, 0.33 amps/watt. Receiver parameters are: aperture, 20 mm; and acceptance angle, 1.82° .

The transmissometer electronics, shown schematically in Figure 2, supplies regulated power, generates a modulated-temperature compensated drive voltage to the LED and synchronously detects the amplified detector signal.

Power requirements for the transmissometer are 8 to 15 VDC at approximately 10 milliamperes, which is normally supplied by a 12 VDC lantern battery. Power is fed through a blocking diode D1 to prevent damage to the circuitry in case reverse polarity is applied to the power terminals. The +7.5 V regulated supply consists of FET-Q1, operational amplifier - A2A, a 2.5 VDC reference-VR and resistors - R1 and R2. An astable multivibrator IC1, in conjunction with FET switch - IC2 and the diode rectifier filter (D2, D3, C5, C6) generate a negative voltage which is regulated to -2.5 VDC by A2B, R3, and R4.

LED drive voltage is supplied by A1B through R13. The input signal to A1B is the sum of the +2.5 VDC reference voltage (VR) and the negative output from the temperature compensation circuit - A1A, D5, R6. The resistor divider ratio of R7, R8, and R9 is adjusted to temperature compensate the radiated output power of the LED. Modulation of the LED output is accomplished by switching the gain of A1B with a FET switch in IC2.

The detector output current is amplified by the current to voltage converter - A3A, R14, C7, and then A.C. coupled by capacitor C8 to remove any D.C. component in the received signal caused by ambient light incident on the detector. Amplifiers A4B and A4A then produce "0" degree phase and "180" degree phase signals which are synchronously detected by a SPDT FET switch in IC2. The output from the synchronous detector is then amplified and filtered by A3B, R21, R22, R23, R24, and C9. The output voltage from A3B is calibrated by R24 so that 0 to 5 VDC corresponds to 0 to 100% transmission in water.

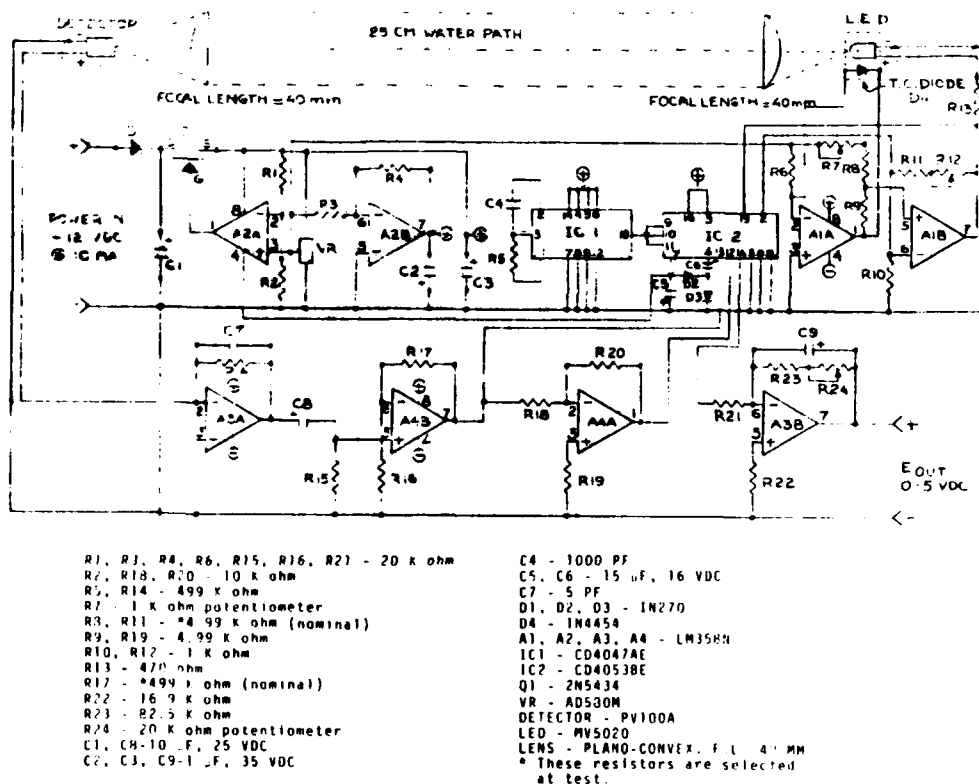


Fig. 2. Transmissometer schematic.

Calibration

Calibration of the transmissometer includes alignment, temperature compensation, and adjustment of the receiver gain to obtain an output voltage corresponding to 90% transmission in filtered distilled water.

Alignment in air is achieved by first collimating the light source so that the transmitted beam at 25 cm is slightly smaller than the receiving aperture and is centered on the receiver lens; the receiver is aligned next to obtain maximum output. During alignment, the LED drive voltage at the output of A1B, is set to 4.5 volts peak. After the light source and optical receiver have been aligned R17 is selected to obtain minus 1 VDC at pin 14 of IC2. The transmissometer is then installed in a temperature control chamber and with R7 and R12 set in the middle of their range, temperature is cycled between 0°C and 25°C. R8 is then selected to temperature compensate the LED and R11 is selected to maintain a 4.5 volt peak drive to the LED at pin 7 of A1B.

After the transmissometer has been aligned and temperature compensated, it is immersed in filtered distilled water, $\beta(45^\circ)$ at $550 \text{ nm} \leq 7 \times 10^{-4} \text{ m}^{-1} \text{ ster}^{-1}$. The transmission of this water was 65.5% as measured by a 1 m beam transmissometer. By applying equation (1) we convert from transmission readings on the 1 m transmissometer, $T(1 \text{ m})$, to readings on the 25 cm transmissometer, $T(0.25 \text{ m})$. Since

$$T(1 \text{ m}) = e^{-c}, \quad c = -\ln T(1 \text{ m})$$

and hence

$$T(0.25 \text{ m}) = e^{(0.25) \ln T(1 \text{ m})}. \quad (2)$$

A reading of 65.5% transmission on the 1 m beam transmissometer is found by means of equation (2) to correspond to a 90.0% transmission reading on the 25 cm transmissometer.

After the instrument has been immersed, the receiver gain, R24, is set so that the output voltage is 4.50 VDC which, for this transmissometer corresponds to 90.0% transmission in water. The unit is then removed from water and the voltage reading in air is recorded

This air reading can be checked periodically to verify that the instrument calibration is stable over a period of time. Three instruments recently were moored by the U.S. Geological Survey for a period of six weeks. Calibration data before and after demonstrate the long term stability (Table 1).

Table 1. Long term stability of the transmissometer data obtained before and after the U.S. Geological Survey mooring.

Date	Unit	Air Calibration (% Transmission)	Zero (% Transmission)	Filtered Distilled Water Calibration (% Transmission)
3-30-78	3	94.8	0.172	90.2
3-31-78	6	90.4	0.008	90.0
3-31-78	8	88.8	0.008	90.2
7-19-78	3	96.6	0.010	89.8
7-19-78	6	89.4	0.008	88.4
7-19-78	8	88.8	0.004	89.6

The transmissometer overall error due to electronics, temperature compensation and instability is less than 0.5%. No evidence of calibration instabilities have been observed due to aging of the LED. This is primarily due to the low drive current (approximately 3 mA average) and the low temperatures (less than 25°C) encountered in natural waters.

Tests were conducted to determine if two instruments would give the same transmission values in natural waters. Sediment collected off the Oregon coast was resuspended in a large stirred water bath with two transmissometers located side by side (Table 2). Between 65 and 90% transmission the two instruments agreed within 0.4%. A 25 cm transmissometer profile has also been compared with one obtained with a one meter path length transmissometer (Figure 3). By means of equation (2) the 1 m transmissometer readings were converted to equivalent readings on the 25 cm transmissometer and plotted for comparison. Tests in daylight and dark have shown that the output is not affected by ambient light.

Table 2. Comparison of two transmissometers in relatively turbid water.

$B(45^\circ) \text{ m}^{-1} \text{ ster}^{-1}$ $\lambda = 550 \text{ nm}$	% Transmission in a 25 cm path $\lambda = 660 \text{ nm}$		Water Type
	Unit 1	Unit 2	
1.0×10^{-3}	90.4	90.4	Distilled
18.4×10^{-3}	79.2	79.6	Distilled + some sediment
54.4×10^{-3}	65.4	65.6	Distilled + more sediment

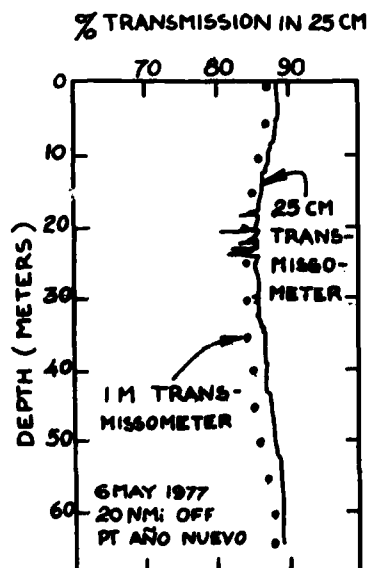


Fig. 3. A comparison of a profile obtained with a 25 cm transmissometer and one obtained with a 1 m transmissometer.

The calibration of an optical instrument in terms of volume or weight of suspended matter must be done experimentally. The attenuation properties of a collection of particles depends on their size, shape and index of refraction structure. The relationship between observed attenuation and particle volume or weight thus changes somewhat as the location of the observation changes. Nevertheless it has been shown (4) that the correlation coefficient between attenuation and suspended volume is .80 to .95 in the surface layer and .90 to .98 below the thermocline. The high correlation indicates that the particle properties do not change a great deal in distances of about 50 miles or in periods of weeks. The exceptions are active phytoplankton blooms, in this case the correlation can be as low as 0.70.

The response of the instrument to a given suspended volume or weight can be calculated approximately as follows. We assume that the particles have a hyperbolic cumulative size distribution $f(D) \propto D^{-C}$, where D is the diameter of the particles. Then we choose $C = 2.9$ and a relative index of refraction of 1.05. Using the Mie scattering tables of Morel (5) one can then calculate that for 1.1×10^{-4} cc/l material we would get a total scattering coefficient $b = .02 \text{ m}^{-1}$ and a volume scattering coefficient at 45° $\beta(45) = 3.4 \times 10^{-4} \text{ m}^{-1} \text{ ster}^{-1}$. If the specific gravity of the material is about 2 g/cc, 100 $\mu\text{g}/\ell$ would yield approximate values of $b = .01 \text{ m}^{-1}$ and $\beta(45) = 1.5 \times 10^{-4} \text{ m}^{-1} \text{ ster}^{-1}$. Since the absorption due to particles is about half of the scattering (6) and absorption and scattering = attenuation, 100 $\mu\text{g}/\ell$ of material in suspension would yield an attenuation coefficient $c = .015 \text{ m}^{-1}$. This number will change somewhat depending on the nature of the material in suspension.

One can calculate the change in transmission in a 25 cm pathlength ($\lambda = 660 \text{ nm}$) due to adding 100 $\mu\text{g}/\ell$ to a suspension. In very clear water ($c = 0.3 \text{ m}^{-1}$ or $T = 74\%$). The change would be, $\Delta T = e^{-(0.3)(0.25)} - e^{-(0.315)(0.25)} \approx 0.5\%$. In very dirty water ($c = 4 \text{ m}^{-1}$ or $T = 2\%$) we get $\Delta T = e^{-(4)(0.25)} - e^{-(4.015)(0.25)} \approx 0.1\%$. In the clearest water the instrument can thus detect changes in particle concentrations of 100 $\mu\text{g}/\ell$, which is as good or better than a typical $\beta(45)$ scattering meter with a resolution of $2 \times 10^{-4} \text{ m}^{-1} \text{ ster}^{-1}$. In very turbid water ($C = 4 \text{ m}^{-1}$) a change of 0.5% in transmission requires a change in beam attenuation of about 0.6 m^{-1} or about 4000 $\mu\text{g}/\ell$. Due to the exponential nature of transmission losses the instrument is thus more sensitive to changes in particle concentration in clean water.

Results

The instrument has been field tested in a variety of locations and conditions. Figure 4 shows some results from a cruise between Oregon and Peru on which simultaneous measurements of diffuse attenuation and beam transmission were made. Figure 5 shows a transmission profile taken in a fresh water reservoir in Oregon. Figure 6 displays results from a mooring on the Oregon shelf in which the transmissometer was used in conjunction with a current meter in order to study sediment resuspension and transport. The instrument has also been moored for periods up to 6 weeks with satisfactory results.

Data Interpretation

Part of the error in a transmission measurement is due to the inclusion of forward scattered light. If $\beta(\theta)$ is the volume scattering function and γ is the half angle of the receiver, the attenuation coefficient will be underestimated by $g = 2\pi\gamma \int \beta(\theta) \sin\theta d\theta$. The measured transmission will then be overestimated by a factor of e^{-g} . In this transmissometer $\gamma = 1.8^\circ$. It has been shown (7) that the volume scattering function for angles less than 1.8° is flat as predicted by Mie (3) theory. We can thus integrate $\beta(\theta)$ to obtain g as shown on Table 3. Table 3 also shows what the beam attenuation coefficient is for a given near forward scattering function, β_f , when the slope of the hyperbolic particle size distribution is 2.9 and the index of refraction is 1.05. For different types of particles, the beam attenuation will be different, but of the same order of magnitude. It is thus possible to correct for the finite half angle of the receiver if either the forward scattering is known or if the nature of the particles is known. If neither is known one can use the results in Table I as representing average oceanic conditions. The error due to this effect is always in the same direction as the amount of light received is always larger than it should be. Applying an average correction is thus better than applying no correction at all.

Acknowledgments

This work was supported by the U.S. Geological Survey under contract 14-08-0001-16817 and by the Office of Naval Research contract N00014-76-C-0067 under project NR 083 -102. The support of these agencies is gratefully acknowledged. We are indebted to Mark Matsler of Griffio Brothers Ironmongers for his help in the mechanical design and the machining of the transmissometer. We thank Gail Henwood for typing the manuscript, Rick Spinrad and Terry Chriss for their efforts in obtaining the data presented in this paper, and Dave Menzies and Walt Dillon for critical readings of the manuscript.

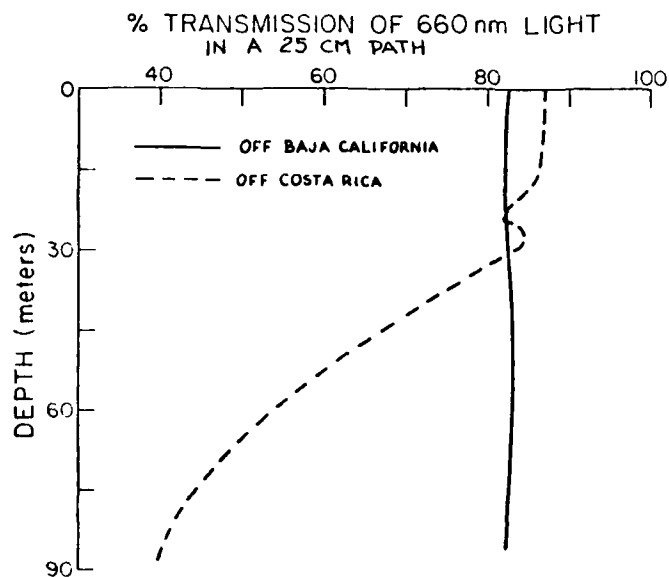


Fig. 4. Measurements taken with the 25 cm transmissometer off Costa Rica and Baja California.

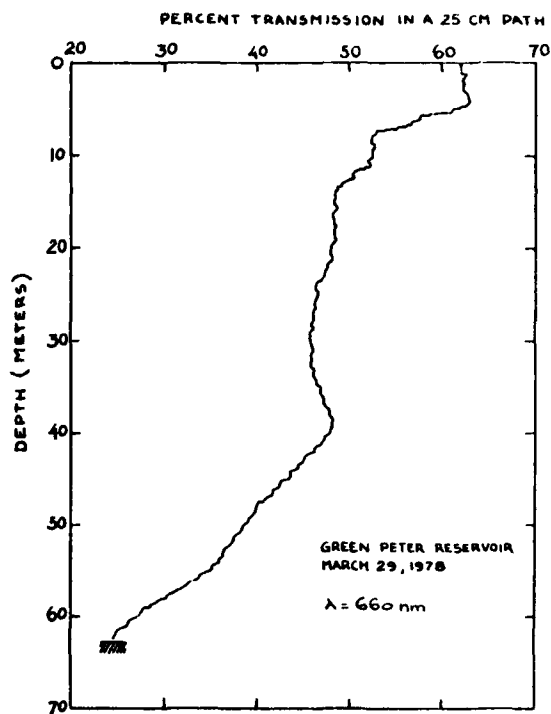


Fig. 5. Transmissometer profile taken in Green Peter Reservoir, Oregon.

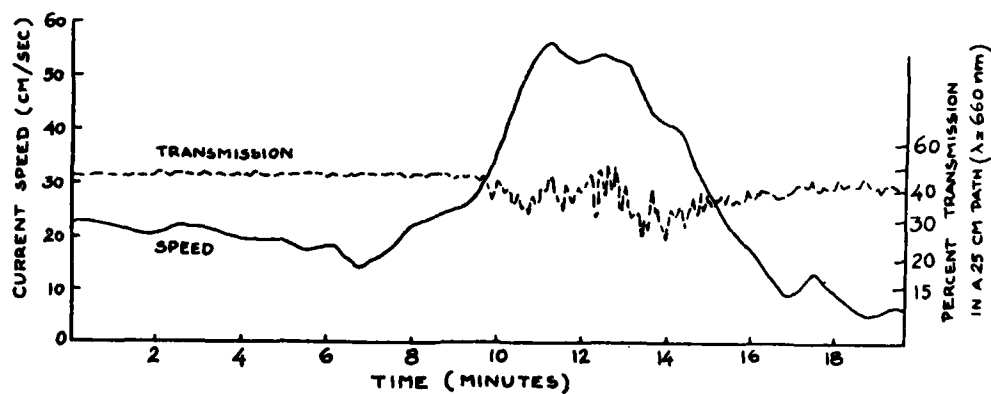


Fig. 6. Transmission in a 25 cm path and current speed as measured off the Oregon coast in about 60 m water depth and 1 m above the bottom.

Table 3. The percent error by which the transmissometer overreads when the volume scattering function between 0° and 1.8° is given by β_f . The beam attenuation coefficient, c , corresponding to β_f , for a hyperbolic particle size distribution with a slope of 2.9 and index of refraction relative to water of 1.05 is also given.

β_f (m^{-1} ster $^{-1}$)	1.0	10.0	50.0	100.0	250.0	500.0	750.00	1000.0
c (m^{-1}) for slope = 2.9 $m = 1.05$	0.01	0.11	0.56	1.13	2.83	5.65	8.48	11.30
% error in transmission reading	0.077	0.77	3.80	7.46	17.62	32.13	44.08	53.93

References

1. Kitchen, J. C., J. R. V. Zaneveld, and H. Pak, "The vertical structure and size distributions of suspended particles off Oregon during the upwelling season", Deep-Sea Res., Vol. 25, pp. 453-468. 1978
2. Pak, H. and J. R. V. Zaneveld, "Bottom nepheloid layers and bottom mixed layers observed on the continental shelf off Oregon", J. Geophys. Res., Vol. 82, pp. 3921-3931. 1977.
3. Mie, G., "Beiträge zur Optik trüber Medien, speziell kolloidalen Metall-lösungen Ann. Phys., Vol. 25, p. 377.
4. Peterson, R. L., A Study of Suspended Particulate Matter: Arctic Ocean and Northern Oregon Continental Shelf, Ph.D. Dissertation, Oregon State University, 122 pp. 1977.
5. Morel, A., "Indicatrices de Diffusion Calculees par la Theorie de Mie pour les Systemes Polydisperses in Vue de l'Application aux Particules Marines." Rapport no. 10, Laboratoire d'Océanographie Physique (Université de Paris VI - CNRS) 73 pp. 1973
6. Jerlov, N. G., "Marine Optics." Elsevier Oceanog. Series No. 14, Elsevier Scientific Publishing Co., Amsterdam-Oxford-New York, 231 pp, 1976.
7. Spinrad, R., J. R. V. Zaneveld, and H. Pak, "Volume scattering functions of suspended particulate matter at near-forward angles: a comparison of experimental and theoretical values", Applied Optics, Vol. 17, pp. 1125-1130. 1977.

FILME

2-84

DTIC